JNeurosci
THE JOURNAL OF NEUROSCIENCE

*Research Articles: Behavioral/Cognitive*

# Network communications flexibly predict visual contents that enhance representations for faster visual categorization

https://doi.org/10.1523/JNEUROSCI.0156-23.2023

**Cite as:** J. Neurosci 2023; 10.1523/JNEUROSCI.0156-23.2023

Received: 25 January 2023
Revised: 25 May 2023
Accepted: 30 May 2023

# Network communications flexibly predict visual contents that enhance representations for faster visual categorization

**Abbreviated title: Networks to Predict and Categorize Visual Contents**

Yuening Yan[1], Jiayu Zhan[2], Robin A.A. Ince[1], & Philippe G. Schyns[1*]

[1] School of Psychology, University of Glasgow, 62 Hillhead Street, G12 8QB, Glasgow

[2] School of Psychological and Cognitive Sciences, Peking University, 5 Yiheyuan Road, Beijing

***Corresponding author: Philippe G. Schyns** Philippe.Schyns@glasgow.ac.uk

**Keywords:** Brain network; top-down prediction; visual categorization; prefrontal mediation

**This manuscript includes** Main Text**,** Figures 1 to 10, Tables 1 to 2

**Number of words:** Abstract (204), Introduction (291), Discussion (1186).

**Declaration of interests:** The authors declare no competing interests.

**Acknowledgements:** P.G.S. received support from the Wellcome Trust (Senior Investigator Award, UK; 107802) and the Multidisciplinary University Research Initiative/Engineering and Physical Sciences Research Council (USA, UK; 172046-01). R.A.A.I. was supported by the Wellcome Trust [214120/Z/18/Z]. The funders had no role in study design, data collection and analysis, decision to publish or preparation of the manuscript.

## Abstract

Models of visual cognition generally assume that brain networks predict the contents of a stimulus to facilitate its subsequent categorization. However, understanding prediction and categorization at a network level has remained challenging, partly because we need to reverse engineer their information processing mechanisms from the dynamic neural signals. Here, we used connectivity measures that can isolate the communications of a specific content to reconstruct these network mechanisms in each individual participant (N=11, both sexes). Each was cued to the spatial location (left vs. right) and contents (Low vs. High Spatial Frequency, LSF vs. HSF) of a predicted Gabor stimulus that they then categorized. Using each participant's concurrently measured MEG, we reconstructed networks that predict and categorize LSF vs. HSF contents for behavior. We found that predicted contents flexibly propagate top-down from temporal to lateralized occipital cortex, depending on task demands, under supervisory control of prefrontal cortex. When they reach lateralized occipital cortex, predictions enhance the bottom-up LSF vs. HSF representations of the stimulus, all the way from occipital-ventral-parietal to pre-motor cortex, in turn producing faster categorization behavior. Importantly, content communications are subsets (i.e. 55-75%) of the signal-to-signal communications typically measured between brain regions. Hence, our study isolates functional networks that process the information of cognitive functions.



## Significant Statement

An enduring cognitive hypothesis states that our perception is partly influenced by the bottom-up sensory input, but also by top-down expectations. However, cognitive explanations of the dynamic brain networks mechanisms that flexibly predict and categorize the visual input according to task-demands remain elusive. We addressed them in a predictive experimental design, by isolating the network communications of cognitive contents from all other communications. Our methods revealed a Prediction Network that flexibly communicates contents from temporal to lateralized occipital cortex, with explicit frontal control, and an occipital-ventral-parietal-frontal Categorization Network that represents more sharply the predicted contents from the shown stimulus, leading to faster behavior. Our framework and results therefore shed a new light of cognitive information processing on dynamic brain activity.

# Introduction

Since Helmholtz's "unconscious inferences", vision scientists have worked with the hypothesis that what we visually perceive is influenced by the bottom-up sensory input, but also by top-down expectations of what this input might be (Kinchla and Wolfe, 1979; De Lange et al., 2018). Expectations predict upcoming visual information contents (Yuille and Kersten, 2006; Friston, 2010; Clark, 2013), thereby facilitating their disambiguation from the noisy input (Gilbert and Sigman, 2007; Kok et al., 2012) to speed up categorization behavior (Bar et al., 2006).

Studies of the dynamic predictive brain have mainly focused on how predictions can top-down modulate neural signals. For example, predictions can induce patterns of local stimulus-specific activation, in hippocampal, ventral temporal, and primary visual cortex (Kok et al., 2014, 2017; Hindy et al., 2016; Margalit et al., 2020), or enhance gamma and reduce low-alpha oscillations in visual and frontal cortex (Benedek et al., 2011; Haegens et al., 2011; Michalareas et al., 2016; Lobier et al., 2018). Predictions can also enhance high-alpha synchronization in the frontal-parietal-occipital network (Lobier et al., 2018). However, key to understanding the mechanisms that top-down predict visual contents to facilitate their bottom-up categorizations is to reconstruct, from such neural signal modulations, the elusive network that process (i.e. predict and categorize) specific information depending on the demands of the cognitive tasks. To address these points, we reverse engineered 1) the Prediction Network that top-down communicates specific stimulus contents, before the stimulus is shown, to the expected contra-lateral occipital hemisphere, and 2) the Categorization Network, that bottom-up processes these predicted contents from the stimulus to speed up its categorization.

Specifically, our research addresses three fundamental information processing questions pertaining to the prediction and categorization of visual contents (illustrated in Figure 1):

1) When, where, and how does a Prediction Network of brain regions flexibly represent and communicate the predicted contents of a stimulus?

2) When, where, and how does a Categorization Network represent and communicate these contents when presented in the stimulus for behavior?

3) How do predicted contents in (1) change stimulus content in (2) to speed up categorization behavior?

[FIGURE 1]

# Materials and Methods

### Participants

Eleven participants (18-35 years old, mean=26.8, SD=3.0, 4 males and 7 females) took part in the experiment and provided informed consent. All had normal or corrected-to-normal vision and reported no history of any psychological, psychiatric, or neurological condition that

might affect visual or auditory perception. The University of Glasgow College of Science and Engineering Ethics Committee approved the experiment (Application Number: 300210118).

**Stimuli**

Stage 1 of the experimental design (see Figure 2) used two location cues (one for left- and one for right-cued trials). Stage 2 used 3 different sweeping sounds, serving as LSF, HSF and neutral auditory cues. Stage 3 used 2 locations × 2 spatial frequencies × 3 orientations Gabor patches as stimuli. We detail them below.

Stage 1 Location Cues

Participants sat at a 182 cm viewing distance from the screen. We presented a green dot of 1 deg of visual angle diameter for 100 ms to the left (vs. right) of a fixation cross (2 deg of visual angle eccentricity).

Stage 2 SF Cues

Three 250 ms sweeping sounds started with auditory frequency of 196Hz (cueing LSF), 2217Hz (cueing HSF) or 622Hz (no prediction), with a sweep rate of 0.5 rising octave/second.

Stage 3 Gabor Stimuli

Left (vs. right)-cued Gabor patches were presented (diameter, 7.5 visual degrees; left and right eccentricity, 12.5 visual degree), with LSF (vs. HSF) contents of 0.5 cycle/degree (vs. 1.2 cycle/degree) shown at one of three randomly chosen orientations (-15 deg, 0 deg, +15 deg). Prior to the task, we calibrated the LSF and HSF Gabor contrast independently for each participant, using an adaptive staircase procedure (target accuracy set at 90%). On each calibration trial, a left (vs. right) green dot presented for 500ms predicted the upcoming left vs. right location of the LSF or (HSF) Gabor patch, itself presented for 100ms. Participants responded “LSF” vs. “HSF” vs. “don’t know” without feedback. We adaptively adjusted LSF vs. HSF contrast as follows:

$$Contrast = Contrast - 1*(Correct\ vs.\ Incorrect - target\ accuracy)/Shifting\ Count,$$

where *Shifting Count* counts the number of direction changes (i.e., increasing to decreasing, or decreasing to increasing). The adaptive staircase stopped when the adjustment step was < 0.01, setting each SF contrast for this participant’s Gabor stimuli in the actual experiment.

**Procedure**

Each three-stage trial started with a central fixation cross presented for 500ms (Figure 2A accompanies the description below):

Stage 1. A green dot presented for 100ms appeared to the left or right of the central fixation cross, predicting the left vs. right location of the upcoming Gabor with a validity of 1. This was followed by a jittered blank screen [1000-1500ms].

Stage 2. Three sweeping sounds presented for 250ms predicted the Gabor stimulus presented at Stage 3. On, predictive trials, the 196Hz (vs. 2217Hz) sound predicted the upcoming LSF (vs. HSF) Gabor (both with .9 validity). The 622Hz sound was a neutral cue

without predictive value. This neutral cue was followed by LSF vs. HSF Gabors with .5 probability, on 33% of the trials (neutral trials).

Stage 3. The LSF vs. HSF Gabor stimulus appeared at one of the three rotations on the left vs. right screen location for 100ms. The Gabor was either LSF or HSF, with one of three randomly chosen orientations, followed by a 750 to 1,250ms inter-trial interval (ITI) with jitter. We instructed participants to respond "LSF" vs. "HSF" vs. "Don't know" as quickly and as accurately as they possibly could. They did not receive feedback. We counterbalanced the use of the three keys (i.e., LSF, HSF, don't know) across participants, which helped to minimize any effect from specific fingers.

The experiment comprised several blocks of 54 such trials (see Table 1 for details). Participants performed 10-14 blocks in a single day, with short break between blocks. They completed the total of 38-45 blocks over 3-4 days. Participants completed at least 499 trials in each condition (of left vs. right presentation of LSF vs. HSF Gabors). Participants learned the correct relationships between the auditory cues and predicted SF within ~2 blocks of trials, without explicit instructions. We therefore removed these first two blocks from all subsequent analyses.

[TABLE 1]

Auditory localizer. Prior to the experiment, we ran an MEG localizer to model the bottom-up processing of each one of 3 auditory cues. For each cue, each localizer trial started with a blank screen for 500ms, followed by the auditory tone for 250ms, then a blank screen for 1250ms ITI. In a block of 12 trials, 10 of the trials presented the same tone and the two other tones were catch tones. Participants had to press a key whenever the tone was a catch tone. Each participant completed 36 such blocks (i.e., 12 blocks per type of tones), with block order of "low frequency", "middle frequency", "high frequency", repeated 12 times.

**MEG Data Acquisition and Pre-processing**

We measured participants' MEG activity with a 248-magnetometer whole-head system (MAGNES 3600WH, 4-D Neuroimaging) at a 508Hz sampling rate. We performed the analysis according to recommended guidelines using the FieldTrip toolbox (Oostenveld et al., 2011) and in-house MATLAB code.

For each participant, we discarded the runs (i.e., blocks) with the head movements more than 0.6cm, measured by pre-run vs. post-run head position recordings. We then applied a 1Hz high-pass filter ($5^{th}$ order two-pass Butterworth IIR filter) to the remained data, and removed the line noise using discrete Fourier transform. We epoched the raw data into trial windows, separately for each stage: Stage 1, -200ms pre-dot onset to 1,000ms post-dot onset (henceforth [-200ms 1,000ms] around onset); Stage 2: [-200ms 1,000ms] around sweeping sound onset; Stage 3: [-200ms 600ms] around Gabor patch onset. We de-noised the epoched data via a PCA projection of the reference channels. We rejected noisy channels with a visual selection and rejected jump and muscle artifacts with automatic detection(Oostenveld et al., 2011). We decomposed the output dataset with ICA, identified and removed the independent components corresponding to artifacts (eye movements, heartbeat—i.e. 2-4 components per participant).

**Source Reconstruction**

For each participant, we co-registered their anatomical MRI scan with their head shape recorded on the first session and normalized the volume data to standardized MNI coordinate space(Gross, 2019). Using brain surfaces segmented from individual warped MRI, we then prepared a realistic single-shell head model. We resampled each epoched dataset (i.e., each stage) at 512 Hz, low-pass filtered the data at 25Hz ($5^{th}$ order Butterworth IIR filter), specified the time of interest between 0-500ms (post cue at Stage 2; post Gabor stimulus at Stage 3) and computed covariance across the entire epoch. We then computed the forward model with a 6mm uniform grid warped to standardized MNI coordinate space, and performed the Linearly Constrained Minimum Variance Beamforming (LCMV) analysis to reconstruct the time series of each source, with parameter 'lambda=6%'. Following the above steps, for each participant we obtained single-trial time series of 4,413 MEG cortical sources at a 512Hz sampling rate between 0 and 500ms that we used to analyze the dynamic information processing in the Prediction and Categorization Networks—i.e. at Stages 2 and 3, see Figure 1.

We applied the same pre-processing pipeline to the MEG localizer, using the epoched data [-200ms 500ms] around tone onset. We applied the LCMV analysis 0-500ms post tone, to reconstruct the source representation of the MEG localizer data.

**Analyses**

***Cueing improves behavior***

At a group-level, we discarded invalid predictive trials and applied a 2 (left vs. right location cues) × 2 (valid predictive vs. neutral cueing) × 2 (LSF vs. HSF Gabor patches) ANOVA on the median RTs (excluding incorrect response and outliers) and on the accuracy of all participants. We found a significant main effect of valid predictive vs. neutral SF cueing on RTs, showing that valid predictive trials are significantly faster than neutral trials ($F(1,10)$=20.8, $p$=0.001); and a significant interaction effect between location cue and Gabor SF ($F(1,10)$=17.4, $p$=0.002). Further analysis showed that this predictive vs. neutral cueing effect is significant ($p$<0.05, after Bonferroni correction) for each of the 4 experimental conditions (left vs. right locations × low vs. high SFs), quantified by a paired-sample t-test, independently for each condition. For categorization accuracy (ACC), the ANOVA was significant only for valid predictive vs. neutral cueing, showing that ACC is significantly higher in valid predictive than neutral trials ($F(1,10)$=22.5, $p$=0.0008); and a significant interaction between location cue and Gabor SF ($F(1,10)$=13.8, $p$=0.004). Further analysis showed that this effect of SF cue is significant ($p$<0.05, Bonferroni correction) for all but the left-LSF experimental conditions (paired-sample t-test independent for each condition).

***Stage 2: Prediction Network***

*Prediction representations*

To understand the Stage 2 network of regions that propagates the LSF vs. HSF auditory prediction prior to stimulus onset, we computed the representation of the cue across the whole brain, separately for left- and right-cued trials.

For each participant, we computed the single-trial MI(<LSF vs. HSF auditory cue; Stage 2 $MEG_t$>), at each time point from 0 to 400ms following Stage 2 auditory cue onset, on each occipital source (lingual gyrus, cuneus, inferior occipital gyrus), temporal (fusiform gyrus, inferior temporal gyrus, middle temporal gyrus, superior temporal gyrus), parietal (superior

parietal lobe, inferior parietal lobe, angular gyrus, supramarginal gyrus), premotor (precentral gyrus, postcentral gyrus), and frontal (orbitofrontal gyrus, inferior frontal gyrus, middle frontal gyrus, medial frontal gyrus, superior frontal gyrus). We computed MI with the Gaussian Copula Mutual Information (GCMI) estimator(Ince et al., 2017) that supports multi-dimensional variables. This semi-parametric estimator fits Gaussian (maximum entropy) copula, but does not make any assumption about the marginal distributions of the variables.

*Prediction periods clustering*

To compute the number of space x time periods of prediction representations, we applied k-means clustering analysis on all 4413 x 204 (source x time points) dimensional trials as follows:

*Step 1: Peak time extraction.* First, for each participant, and independently for left- and right-cued trials and source, we extracted the peak time MI(<LSF vs. HSF auditory cue; Stage 2 $MEG_t$>), 0 and 400ms post auditory cue onset.

*Step 2: Matrix computation.* Across participants and cued conditions, in each ROI (occipital, temporal, parietal, pre-motor and frontal), we summed the numbers of sources that peak during each 10ms-step time window between 0 and 400ms post auditory cue onset (i.e. 39 time windows), producing a 5 (ROIs) x 39 (time windows) matrix of MI peaks. This matrix represented the total brain volume of prediction representation dynamics over time.

*Step 3: Clustering.* We k-means clustered (k = 1 to 30, repeating 1,000 times) the matrix from Step 2, using the 39 time windows as samples and selected k as the elbow of the within-cluster sums of point-to-centroid distances metric.

The result shows Stage 2, with k = 4 as a good solution, starting with a period 0, before any prediction representation, and then 3 distinct timed periods with temporal, frontal, occipital of peak representations of the prediction.

*Prediction network nodes (supports Figure 3A)*

To reveal the dynamics of MI(<LSF vs. HSF auditory cue; Stage 2 MEG>) representation of the prediction, we localized the source peaking around the first peak in the 90-120ms time window (start), the last peak in 120-200ms (midway) and >200ms (end). We computed the group mean of these 3 source-localized peaks across participants (see Figure 3A for group mean). Further, we applied 2 (left vs. right-cued prediction) * 2 (left vs. right hemisphere) ANOVA on the prediction representation on occipital sources to test the interaction effect (i.e., the contra-lateral effect).

*Prediction network reconstruction (supports Figure 3B)*

To reconstruct the Stage 2 Prediction Network, we computed Directed Feature Information (DFI, where F is the auditory cue predicting the upcoming LSF vs. HSF Gabor) in each participant, for each pair of identified network nodes (i.e., sender: temporal, receiver: frontal; sender: frontal, receiver: occipital) as follows:

*Step 1: Source selection.* We selected the highest MI source for the sending and receiving regions in the time window of interest (temporal: 90-120ms, frontal: 120-200ms, occipital: >200ms).

*Step 2: Directed Information (DI).* DI (i.e. event-related Transfer Entropy) quantifies all the information communicated from sending to receiving sources, removing information sent from the receiver itself. For the receiver at time $x$, with a communication delay $y$ from the sender, DI is computed as the Conditional Mutual Information (CMI) between $RA_x$ and $SA_{x-y}$ conditioned on $RA_{x-y}$:

$$DI = CMI<RA_x; SA_{x-y}|RA_{x-y}> \quad (1)$$

Thus, we computed DI between each sender and receiver source, for each receiver time point between 0 and 400ms post auditory cue onset, and for each communication delay between 0 and 300ms. This produced the receiver-time × transfer-delay DI matrix.

*Step 3: DI conditioned on Feature (DI|F).* DI|F removes from DI the information communicated about the predictive LSF vs. HSF feature itself. We computed DI|F for each receiving-time × communication-delay.

*Step 4: DFI.* The difference between DI and DI|F isolates the information communicated about the predictive cue. We computed DFI as:

$$DFI = DI - DI|F \quad (2)$$

for each receiving-time × communication-delay cell of the matrix.

*Step 5: Statistical significance.* We repeated 200 times DFI computations with shuffled feature labels (i.e., LSF vs. HSF), using as statistical threshold the 95$^{th}$ percentile of the distribution of 200 maxima (each taken across the DFI matrix of each shuffled repetition, FWER, $p$<0.05, one-tailed).

*Step 6: Communication proportions*. To compute the proportion of communications about a feature in total network communications between two regions, we computed ratio DFI/DI, at the maximum receiving-time × communication-delay of the DFI measure.

We applied Step 1-6 to reconstruct the Stage 2 Prediction Network of each individual participant. Figure 8 shows the individual participants' DFI networks; Figure 3B shows the group average network. Note here we established the same statistical significance test for each participant and reported a combination of frequentist and Bayesian estimation(Ince et al., 2021a). The Bayesian approach contains a two-level analysis, where the first-level analysis involves null hypothesis significance testing (NHST) within participants and the second level is the Bayesian estimation of population prevalence.

*Prediction network mediation (supports Figure 4)*

We then tested whether frontal cortex is a necessary mediator of Stage 2 prediction communications between temporal and occipital cortex, by isolating the role of the frontal region in these communications. We then compared network communications with and without frontal mediation. The steps below detail how we computed frontal mediation in the Prediction Network of each participant.

*Step 1: Frontal Mediation, DFI.* On the selected temporal and occipital sources, for receiving time points between 0 and 400ms post auditory cue onset and for each delay between 0 and 300ms, we computed the receiving-time × communication-delay of temporal-to-frontal DFI and then frontal-to-occipital DFI (each computed as in *Prediction network*

298 *reconstruction*). This quantifies the mediating role of the frontal region in the communication
299 of the predictive cue (cf. Figure 4B).

300 *Step 2: Direct Communication, DFI|Frontal.* To isolate the role of frontal mediation,
301 we also computed temporal-to-occipital DFI conditioned on the frontal activity. Specifically,
302 for each time point in the combination of (1) receiving time *x* between 0 and 400ms post
303 auditory cue onset (2) communication delay *y* between 0 and 300ms (3) and mediation time
304 *z* between receiving time and sending time (i.e., *x* and *x-y*), we computed DFI received by
305 occipital at time *x*, sent by temporal at *x-y*, conditioned on frontal activity at time *z*. This
306 produced the 3D DFI receiving-time × communication-delay × mediation-time conditioned
307 DFI matrix. We took the minimum conditioned DFI across the mediation time as the directed
308 communication (i.e., without frontal mediation, Figure 4A).

309 *Step 3: Statistical significance.* We recomputed Steps 1 and 2 and their difference,
310 shuffling the LSF vs. HSF labels—i.e. 200 repetitions, using the 95$^{th}$ percentile of 200
311 maxima as statistical threshold, each maximum taken across the DFI minus DFI|F matrix of
312 each shuffled repetition, FWER, $p<0.05$, one-tailed. This isolated the receiving-time ×
313 communication-delays showing significant enhancement with vs. without frontal mediation.

314 We applied Steps 1-3 to each participant. Figure 4A and B show the results of a typical
315 participant. Figure 9 shows all individual results. Figure 4C shows the group mean difference
316 and its Bayesian prevalence.

317 ***Stage 3: Categorization Network***

318 *Stimulus representations*

319 To reconstruct the Stage 3 Categorization Network, on predictive trials, we computed for
320 each participant the dynamics of LSF vs. HSF Gabor stimulus representation across the
321 whole brain, separately for left- and right-cued trials—i.e. MI(LSF vs. HSF Gabor; Stage 3
322 $MEG_t$), on each source in occipital, temporal, parietal, premotor and frontal regions, at each
323 time point from 0 to 500ms following Gabor onset.

324 *Categorization periods clustering*

325 To compute the number of space x time stimulus representations period, we applied again k-
326 means cross-trials clustering analysis on all 4,413 sources x 256 time points as follows:

327 *Step 1: Peak time extraction.* First, for each participant, and independently for left-
328 and right-cued trials and source, we extracted the peak LSF vs. HSF representation MI in 50
329 10-ms time windows spanning 0-500ms post Gabor.

330 *Step 2: Matrix computation.* Across participants and conditions, we counted the
331 number of sources per ROI (occipital, temporal, parietal, pre-motor and frontal) that peak in
332 each time window, producing a ROI x time matrix of MI peaks.

333 *Step 3: Clustering.* We k-means clustered (k = 1 to 30, repeating 1,000 times) the
334 matrix from Step 2, using the 50 time windows as samples and selected k as the elbow of
335 the within-cluster sums of point-to-centroid distances metric.

336 Stage 3 comprised k = 4 clusters. A first period with no LSF vs. HSF stimulus representation,
337 followed an occipital-ventral (150-250ms, start), parietal (250-350ms), and premotor-frontal
338 (>350 ms) periods of stimulus representation.

*Categorization network nodes* (supports Figure 5A)

To reveal the dynamics of MI(LSF vs. HSF Gabor; Stage 3 MEG), in each participant, we localized the source peaking in each one of the three representational periods. We then computed the group mean of these 3 sources across participants. Figure 5A presents the group mean.

*Categorization network reconstruction* (supports Figure 5B)

To reconstruct the Stage 3 Categorization Network that communicates the Gabor SF across occipital, parietal, premotor regions identified earlier, we computed DFI communications of the LSF vs. HSF stimulus information. That is, in each participant, for each pair of regions (i.e., sender: occipital, receiver: parietal; sender: parietal, receiver: premotor), we performed the following three steps.

*Step 1: Source selection.* We selected one sender and one receive source with highest Stage MI representation of Gabor LSF vs. HSF in the time window of interest (occipital: 150-250ms, parietal: 250-350ms, premotor: >350ms).

*Step 2: DFI.* For each receiver time points between 0 and 500ms post Gabor stimulus onset, and for each sender delays between 0 and 300ms, we computed the receiver-time × communication-delay of LSF vs. HSF stimulus representation with DFI (see specific computations in *Prediction network reconstruction)*.

*Step 3: Statistical significance* was established recomputing DFI with shuffled LSF vs. HSF labels—i.e. 200 repetitions, using as statistical threshold the 95$^{th}$ percentile of 200 maxima, each taken across the DFI matrix of each shuffled repetition, FWER, $p$<0.05, one-tailed.

*Step 4: Communication proportions*. To compute the proportion of communications about a feature in total network communications between two regions, we computed ratio DFI/DI, at the maximum receiving-time × communication-delay of the DFI measure.

We applied Steps 1-4 in each participant, reconstructing the occipital-to-parietal and parietal-to-premotor network that communicates the LSF vs. HSF Gabor contents (Figure 10 shows all individual results; Figure 5B shows the group average).

***Stage 2 to Stage 3: Influences of Prediction Network on Categorization Network***

*Prediction enhances stimulus representation (supports Figure 6A)*

To understand how Stage 2 predictions of LSF vs. HSF facilitate their Stage 3 categorization when the stimulus is shown, we compared LSF vs. HSF Gabor representations between Stage 3 valid predictive and neutral trials, in each participant and Categorization Network region (i.e., contra-lateral occipital-ventral, parietal, premotor). Specifically, we computed MI as follows:

Step 1: *Source selection.* We selected one Stage 3 source per region with highest MI(LSF vs. HSF Gabor; Stage 3 $MEG_t$ ) during the time window of interest (occipital-ventral: 150-250ms; parietal: 250-350ms; premotor: >350ms).

Step 2: *MI computation.* For each selected source, we computed source-by-time MI(LSF vs. HSF Gabor; Stage 3 MEG), every 2ms between 0 and 500ms post Gabor onset, separately for valid predictive and neutral trials. For this computation, we matched number of valid predictive trials with neutral trials (random selection). We averaged the MI matrices for valid predictive trials from 5 such random trial selections.

Step 3: *Statistical significance of difference* was established by recomputing the source-by-time MI with shuffled valid predictive and neutral trials (repeated 200 times), calculating the difference of peak between recomputed valid predictive and neutral MI in the time window of interest, using as statistical threshold the 95$^{th}$ percentile of 200 maxima, each taken across the source-by-time difference of each shuffled repetition (FWER, $p$<0.05, two-tailed).

We repeated above Step 1-3 for each participant. Figure 6A shows the group-level results.

*Prediction modulates Categorization Network source activity and RT (supports Figure 6B)*

To demonstrate where and when valid predictions modulate premotor MEG activity to facilitate behavior, we compared the effect of valid predictive vs. neutral at Stage 2 on Stage 3 Categorization Network brain activity and behavioral RT.

Step 1: *Co-Information.* We computed positive Co-I(<predictive vs. neutral; Stage 3 $MEG_t$; RT>), information theoretic redundancy, as follows:

$$\text{Co-I} = MI(\text{<predictive vs. neutral; Stage 3 } MEG_t\text{>}) + MI(\text{<predictive vs. neutral; RT>}) - MI(\text{<predictive vs. neutral; Stage 3 } MEG_t\text{, RT>}),$$

on every source of the Categorization Network and at every 2ms between 0 and 500ms post Gabor onset, producing a vector in Stage 3 time. Specifically, this estimator supports multi-dimensional variables, so the joint information MI(predictive vs. neutral; Stage 3 $MEG_t$, RT) is computed by combining the copula-normalised Stage 3 $MEG_t$, and RT variables into a 2d variable.

Step 3: *Statistical significance* was established by recomputing the Co-I with shuffled predictive vs. neutral labels, 200 repetitions, using as statistical threshold the 95$^{th}$ percentile of 200 maxima, each taken across the vector of each shuffled repetition, FWER, $p$<0.05, one-tailed.

We applied Step 1-3 to each participant. Figure 6B shows the group results.

***Control Analyses***

*Stage 1: Dot Representation*

To check whether representation of the dot cue from Stage 1 remains present until representation of the auditory cue in occipital cortex at Stage 2, we computed the dot cue representation with MI(<left vs. right dot; Stage 1 $MEG_t$>), on each occipital source in lingual gyrus, cuneus and inferior occipital gyrus, at each time point (a) from 0 to 1000 ms following Stage 1 dot cue onset and (b) from -100ms to 0ms around auditory cue onset at Stage 2. We then averaged the time courses of dot representation across the sources. Figure 7A shows the results.

*Stage 2: Auditory Decoding*

We used classifiers trained on auditory localizer data to cross-decode the bottom-up processing of the auditory cues at Stage 2 as follows.

*Step 1: Training.* We trained linear classifiers (MVPA-Light(Treder, 2020)) to discriminate the LSF vs. HSF auditory cue, every 2 ms between 0 and 400ms post stimulus, using MEG sensor responses from the auditory localizer as the training set.

*Step 2: Testing.* Every 2 ms between 0 and 400ms post Stage 2 auditory cue, we computed the classifier decision value from single-trial MEG sensor response. This produced a 2D (training time × testing time) matrix of decision values on each trial. To quantify decoding performance, across trials we computed for each combination of training time and testing time the MI between single-trial classification decision value and the true stimulus label (LSF vs. HSF auditory cue). To establish statistical significance, we repeated the decoding procedure described 1,000 times with shuffled cue labels, applying threshold-free cluster enhancement (TFCE(Smith and Nichols, 2009), $E$=0.5, $H$=0.5), and using as statistical threshold the 95$^{th}$ percentile of 1,000 maximum values (each taken across all the time points per shuffle after TFCE) (i.e., FWER, $p$<0.05, one-tailed). We took the maximum decoding performance across all training time points.

*Step 3: Source representation reconstruction.* At the time point of peak performance, for all 4,413 sources, we computed MI between single-trial decision value and single-trial source activity.

We repeated Steps 1 to 3 to generate the performance curves and source representations of each participant. Figure 7B averages them across participants.

# Results

### 1. Prediction speeds up behavior

Our three-stage cueing design is depicted in Figure 2A. On each trial, a location cue at Stage 1 (green dot) briefly displayed left vs. right of a central fixation cross (Posner cueing(Posner and Petersen, 1990)) predicted the visual hemifield location (left vs. right) of an upcoming Gabor patch (henceforth, Gabor, see *Methods, Stimuli*) with 100% validity, followed by a 1-1.5s blank screen. Stage 1 introduced a left vs. right hemisphere task-demand that a flexible prediction pathway should accommodate. At Stage 2, all trials started with an auditory cue. On “predictive” trials (66% of total), a 250ms sweeping tone (196 Hz vs. 2217 Hz) signalled the Spatial Frequency content (SF, Low vs. High, with an equal split of trial numbers) of the upcoming Gabor stimulus with 90% validity. On “neutral” trials (33% of total), a 622Hz tone had no association with the upcoming stimulus. The auditory cue was followed by another 1-1.5s blank interval (“prediction period”). Figure 2B depicts the couplings between auditory cues and Gabors. Finally, at Stage 3, one of two (LSF vs HSF) Gabor stimuli appeared in the participant’s left or right visual hemifield for 100ms, with fixed brightness and contrast. Each participant (N = 11, see *Methods, Participants*) categorized the Gabor SF as quickly and accurately as they possibly could without feedback (i.e. 3-AFC, with responses “LSF” vs. “HSF” vs. “don’t know”, see also *Methods, Procedure*).

[FIGURE 2]

As expected, SF prediction (in valid, predictive trials) improved categorization accuracy (compared to neutral trials), on average by 2.58% (96.9% vs. 94.3%), *F(1,10)*=22.5, *p*=0.0008, and sped up Reaction Times (RTs), on average by 87.7ms (454.4ms vs. 542.1ms), *F(1, 10)*=20.8, *p*=0.001. Significant RT improvements applied to each Gabor location × SF presentation condition (see Figure 2C, and Table 2 and *Methods, Cueing improves behavior*) and individual participant – i.e., Bayesian population prevalence(Ince et al., 2021b, 2022), with maximum a posteriori probability (MAP) estimate of the population prevalence of the effect of 11/11 = 1 (95% highest posterior density interval, HPDI [0.77 1]). That is, this experiment provides evidence that this within-participant result generalises to most individuals, if they participated in the same experiment.

[TABLE 2]

This speeding up of categorization behavior following prediction should involve the information processing mechanisms of a flexible, task-demand sensitive Prediction network at Stage 2 and a Categorization Network at Stage 3. To understand where, when and how their mechanisms led to faster RTs, we reconstructed and analyzed these networks in each participant (from 4,413 MEG sources covering the whole brain, see *Methods, MEG Data Acquisition and Pre-processing*).

**2. Prediction Network**

To identify the brain regions that flexibly communicate the SF prediction over Stage 2, before stimulus onset (cf. Figure 1), we computed how strongly each MEG source dynamically represents the prediction, separately for left- and right-cued trials at Stage 1 (to reveal lateralization of prediction communication into occipital cortex(Flom et al., 1963) at Stage 2).

Specifically, for left- and right-cued trials at Stage 1, we computed the Stage 2 spatial-temporal representation of the predictive SF auditory cue and MEG source activity using Mutual Information(Ince et al., 2017)–i.e. MI(LSF vs. HSF auditory cue; Stage 2 $MEG_t$), over 4,413 MEG sources, every 2ms between 0 and 400 ms post Stage 2 cue onset, see *Methods, Prediction representations*. In each participant, this computation produced two source-by-time matrices (for left- and right-cued trials at Stage 1) whose MI values indicate the strength of SF prediction representation at Stage 2.

To reveal the spatial-temporal unfolding of prediction representation, we applied a data-driven clustering analysis to these MI matrices (see *Methods, Prediction periods clustering*). We found three distinct spatial-temporal periods (i.e. clusters) in both left- (see Figure 3A, first row) and right-cued trials (see Figure 3A, second row). Figure 3A summarizes their dynamics at group level, by plotting the sources with maximal Stage 2 prediction

representation (i.e. peak MI) in each color-coded period. These periods replicated in each individual participant.

Specifically, Figure 3A shows that Stage 2 prediction representation dynamics start with an early Temporal Lobe (TL) peak (auditory cortex, blue, Period 1), moving to prefrontal cortex (dorsal lateral PFC, [120-200ms], magenta, Period 2), and then finally to the occipital cortex (OC) contra-lateral to the predicted location ([>200ms], orange, Period 3). Of note, Stage 2 prediction representations were contra-lateralized on occipital sources–i.e. to the Stage 1 cued spatial location, group-level ANOVA, 2 (left vs. right prediction) by 2 (right vs. left hemisphere occipital cortex), $F(1, 10) = 18.87$, $p = 0.0015$), replicated in 10/11 participants, Bayesian population prevalence = 0.91 [0.64 0.99], MAP [95% HPDI].

[FIGURE 3]

The dynamics of prediction propagation suggest a functional network that specifically communicates the predictive cue. Reconstructing this network requires quantifying the communication of the predictive information separately from all other communications. We did this by computing Directed Feature Information (DFI) (Ince et al., 2015a), which quantifies directed, time-lagged region-to-region communication about a specific feature (here, the predictive cue). We computed DFI (of LSF vs. HSF prediction, henceforth P) between pairings of the three sources identified earlier (i.e. one per color-coded period, that is, temporal, prefrontal and occipital), for each possible time lag, and separately for left- and right-cued trials–i.e. $DFI_P(regionA_{t1} \rightarrow regionB_{t2})$, see *Methods, Prediction network reconstruction*.

Figure 3B shows these prediction communications as the cross-participant DFI matrix between sender (y-axis) and receiver sources (x-axis), across different time delays (FWER-corrected, $p<0.05$, one-tailed), in right-cued trials. The PFC source (x-axis, left panel) receives the predictive cue ~160ms, sent from the temporal TL source ~50ms earlier (y-axis, right panel); PFC then flexibly sends the predictive cue (y-axis, right panel) contra-laterally to left occipital (lOC) sources on right-cued trials (x-axis, right panel), with a 100-200ms delay. We replicated these communications in individual participants as follows (see prevalence bar in Figure 3B): TL->PFC: left-cued trials (unfilled) 11/11, right-cued (filled) trials 11/11, Bayesian population prevalence = 1 [0.77 1] MAP [95% HPDI]; PFC->rOC: left-cued trials, 9/11, Bayesian population prevalence = 0.81 [0.53 0.96], MAP [95% HPDI]; PFC->lOC: right-cued trials,10/11, Bayesian population prevalence = 0.91 [0.64 0.99], MAP [95% HPDI], see Figure 7 for individual results.

Importantly, we found that SF communications in the Prediction Network comprise only a percentage of the total region-to-region communications (calculated by Directed Information(Massey, 1990), see *Methods Prediction network reconstruction Step 3 and 6*). These results emphasize the importance of isolating communications of contents–i.e. across participants, 74.2±13.1% of temporal-to-prefrontal for left-cued trials, 69.4±19.0% for right-

cued trials; 60.3±19.0% of prefrontal-to-occipital communications, left-cued trials, and 67.1±22% for right-cued trials.

We now know that PFC flexibly communicates the prediction from TL to lateralized OC, depending on task-demand stimulus location at Stage 1. We also know that prefrontal cortex synchronises with visual cortex (signal-to-signal) in top-down visual predictions tasks (Bar et al., 2006; Lobier et al., 2018). Now we test the hypothesis that PFC flexibly mediates the communication of prediction contents between TL and OC as a function of task demands. To directly test this mediation, Figure 4 contrasts a direct communication of the prediction from TL to OC, without (vs. with) PFC mediation–i.e. computing $DFI_P(TL_{t1}\rightarrow OC_{t3})|PFC_{t2}$, see Figure 4A (vs. $DFI_P(TL_{t1}\rightarrow OC_{t3})$, see Figure 4B) and *Methods, Prediction network mediation*. Figure 4 reveals that PFC does indeed flexibly mediate the predictive cue from TL to left vs. right OC. That is, these communications are conditional on PFC source activity–and replicated for left- and right-cued trials in ≥ 10/11 participants, see Figure 8, Bayesian population prevalence = 0.91 [0.64 0.99] (MAP [95% HPDI]). Thus, PFC actively and flexibly mediates the network communications of the prediction from TL to lateralized OC.

[FIGURE 4]

**3. Categorization Network**

Next, we similarly reconstructed the Stage 3 Categorization Network that processes the presented Gabor SF stimulus for behavior. First, on predictive trials, we computed the Stage 3 dynamic representation of the stimulus to identify space-time regions that represent Gabor SF for categorization—i.e. by computing MI(Gabor SF; Stage 3 $MEG_t$), on each source and time point, separately for left- and right-cued trials. Clustering these space-time MI matrices revealed again three periods of Gabor stimulus representation (see Figure 5A and *Methods, Categorization periods clustering*). Specifically, stimulus representation starts with an early lateralized occipital-ventral peak ([150-250ms], orange, Period 4), followed by a parietal lobe peak ([250-350ms], red, Period 5) and a premotor-frontal cortex peak ([> 350ms], brown, Period 6), independently for left- and right-cued trials and replicated in all participants–see *Methods, Categorization Network, Categorization periods clustering*.

Then, we reconstructed in each participant the DFI Categorization Network that communicates the LSF vs. HSF contents–i.e., computed as $DFI(regionA_{t1}\rightarrow regionB_{t2})$, see *Methods, Categorization network* reconstruction. Figure 5B shows that these group-averaged communications develop from contra-lateral occipital-ventral cortex to parietal and then to premotor cortex. We replicated these communications in individual participants as follows (see prevalence bar in Figure 5B): rOC->PL, left-cued trials (unfilled) 10/11, Bayesian population prevalence = 0.91 [0.64 0.99], MAP [95% HPDI]; lOC->PL, right-cued trials (filled) 9/11, Bayesian population prevalence = 0.81 [0.53 0.96], MAP [95% HPDI]; PL->PMC, left- (unfilled) and right-cued (filled) trials 9/11 participants, Bayesian population prevalence = 0.81 [0.53 0.96], MAP [95% HPDI], see Figure 9 for all individual results. Here again, SF feature communications were a proportion of the total region-to-region network communications–i.e. 56.0±27.0% of total occipital-ventral to parietal communications, for

left-cued trials and 62.8±17.7%, for right-cued trials; 59.1±20.5% of total parietal-to-premotor communications for left-cued trials and 56.2±23.2%, for right-cued trials.

[FIGURE 5]

**4. Stage 2 prediction influences Stage 3 stimulus SF representation for faster categorization**

Here, we sought to understand the network mechanisms whereby Stage 2 SF predictions change Stage 3 SF representations from the shown stimulus, leading to faster categorization behavior. We proceeded in two steps, where the first one addresses how prediction changes SF stimulus representation and the second step isolates the Categorization Network components that speed up behavior due to prediction.

**Step 1. Does prediction enhance SF discrimination for categorization?**

We analyzed how Stage 2 SF predictions change Stage 3 stimulus SF representation in each Categorization Network region and participant. Specifically, we computed the difference of SF stimulus representation with and without prediction–i.e. the difference of MI(Gabor LSF vs. HSF; $MEG_{Stage3}$), separately computed for valid predictive and neutral trials (see *Methods, Prediction enhances stimulus representation)*. These representational differences are presented in the boxplots of Figure 6A, in each color-coded space-time region and participant–i.e. on the source that maximizes the difference in this region, against the null hypothesis of no difference, see 0 dash line. Boxplots show that valid predictions enhanced SF discriminations on occipital-ventral (150-250ms), parietal (250-350ms) and PMC (>350ms) sources, FWER, $p<0.05$, two-tailed. 7/11 participants replicated these results in contra-lateral OC, for left- and right-cued trials, Bayesian population prevalence = 0.64 [0.33 0.85] (MAP [95% HPDI]), 9/11 participants in parietal lobe and PMC, Bayesian population prevalence = 0.81 [0.53 0.96], MAP [95% HPDI] (see prevalence bars in Figure 6A).

**Step 2. Where and when does prediction speed up behavioral RT in the Categorization Network?**

Next, we identified the space-time regions of the Categorization Network that relate to faster Stage 3 RT following Stage 2 prediction. In each participant, we computed the Co-Information(valid predictive vs. neutral cue trials; $MEG_{Stage3}$; RT), for each source in the three network regions and separately for left vs. right-cued trials, see *Methods, Prediction modulates source activity and RT*. Co-Information quantifies the influence of prediction that is shared, trial by trial, by MEG and RT. It therefore reveals prediction-related MEG source activity that directly relates to faster RT. Figure 6B plots these results as the participant average of the source with maximal Co-Information at each time point. They reveal two peaks post ~250 ms that maximally relate prediction influence on source activity and faster RT in the Categorization Network at Stage 3. Small brains locate these peaks in the parietal lobe and PMC–replicated in all individual participants, separately for left- and right-cued trials, Bayesian population prevalence = 1 [0.77 1] MAP [95% HPDI].

[FIGURE 6]

In sum, SF Stage 2 predictions enhanced Stage 3 stimulus SF representations in all regions of the Categorization Network, across the time course of processing, though only the parietal lobe and premotor cortex speed up RTs.

**Control analyses and Individual results**

At Stage 2, besides reconstructing Prediction Network, we additionally conducted analyses to control for the potential influence from Stage 1 dot presentation to Stage 2 and the bottom-up processing of the auditory cues. First, we demonstrate in Figure 7A that the Stage 1 dot representation ceases prior to the onset of the auditory cue, providing evidence that the contra-lateralization observed at Stage 2 is not a residual effect from Stage 1. Equally importantly, to control for the bottom-up processing of the auditory cues, we traced their representations at Stage 2 using linear classifier(Treder, 2020) trained to discriminate LSF vs. HSF auditory cues from localizer data. Figure 7B shows their decoding performance. We localized the source contributing to the decoding peaks in each time window of the prediction dynamics. We found that the source representation of the auditory cues remains within TL.

[FIGURE 7]

Importantly, we applied a new approach to statistics where we seek to replicate each result above in each individual participant. We then estimate the Bayesian population prevalence of the results from the experimental sample of participants, thereby alleviating most problems of the replication crisis(Ince et al., 2021a, 2022). Having reported the Bayesian population prevalence, below we show the individual results in detail.

We replicated TL->PFC-OC communications in Stage 2 Prediction Network in individual participants as follows: TL->PFC: left-cued trials (unfilled) 11/11, right-cued (filled) trials 11/11, Bayesian population prevalence = 1 [0.77 1] MAP [95% HPDI]; PFC->rOC: left-cued trials, 9/11, Bayesian population prevalence = 0.81 [0.53 0.96], MAP [95% HPDI]; PFC->lOC: right-cued trials,10/11, Bayesian population prevalence = 0.91 [0.64 0.99], MAP [95% HPDI].

[FIGURE 8]

We replicated the result that TL to OC communications are conditional on PFC source activity for left- and right-cued trials in ≥ 10/11 participants, Bayesian population prevalence = 0.91 [0.64 0.99] (MAP [95% HPDI]).

[FIGURE 9]

We replicated OC->PL->PMC communications in Stage 3 Categorization Network in individual participants as follows (see prevalence bar in Figure 5B): rOC->PL, left-cued trials (unfilled) 10/11, Bayesian population prevalence = 0.91 [0.64 0.99], MAP [95% HPDI]; lOC->PL, right-cued trials (filled) 9/11, Bayesian population prevalence = 0.81 [0.53 0.96], MAP [95% HPDI]; PL->PMC, left- (unfilled) and right-cued (filled) trials 9/11 participants, Bayesian population prevalence = 0.81 [0.53 0.96], MAP [95% HPDI],

[FIGURE 10]

## Discussion

We isolated the network mechanisms that dynamically predict specific visual contents. Then, we examined specifically where, when and how prediction changes stimulus representation to speed up categorization behavior. Our three-stage experimental design used a location cue to predict the left vs. right visual field location of an upcoming Gabor stimulus at Stage 1, to study the effects of prediction on stimulus representation, specifically in the occipital cortex contra-lateral to stimulus presentation, depending on task demands. The Stage 1 location cue was followed at Stage 2 by an auditory cue that predicted the LSF vs. HSF contents of the upcoming Gabor stimulus that appeared on the screen at Stage 3. We reconstructed a Prediction Network that propagates the auditory predictive cue from temporal (90-120ms post Stage 2 cue) to occipital cortex (200-400ms), via prefrontal cortex (120-200ms), all pre-stimulus. We showed that prefrontal cortex (mainly, dlPFC) mediates communication of the predictive cue from temporal to the left vs. right occipital cortex, depending on cued location at Stage 1, demonstrating that the prediction pathway is flexible depending on the demands of the task. When the Gabor stimulus is finally shown at Stage 3, we reconstructed post-stimulus the Categorization Network that propagates the LSF vs. HSF feature from occipital-ventral cortex (150-250ms post Stage 3 Gabor), parietal lobe (250-350ms post Stage 3 Gabor) and premotor cortex (>350ms post Stage 3 Gabor). We then showed how predictions change the Categorization network and found that they enhance LSF vs. HSF representations of the shown stimulus, from occipital cortex to pre-motor cortex, leading to faster behavior. Together, our results quantitatively reveal cognitive network mechanisms that flexibly communicate top-down the prediction of a specific content to occipital cortex, which enhances the bottom-up representation of these contents in the stimulus to speed up behavior.

*Functional networks predict and then represent stimulus contents*

Methodologically, we reconstructed a functional network that flexibly communicates a specific auditory prediction of visual contents (LSF vs. HSF) from temporal to left vs. right occipital cortex, with mediation of the PFC. That is, PFC is necessary to flexibly propagate the predictive cue. Such connectivity analyses involve individual MEG sources acting as sending and receiving network nodes. Importantly, DFI functional connectivity differs from other signal-to-signal connectivity analyses (such as Granger causality or transfer entropy) because DFI isolates what the communication is about (at Stage 2, the auditory prediction of LSF vs. HSF) as a percentage of the full signal-to-signal connectivity (Ince et al., 2015a). At this stage, the specific function of the communications between brain regions that are not about the stimulus features remains to be characterized. They could be about other stimulus

features (e.g. its orientation, or contrast), other aspects of the task (i.e. task engagement) or related to dynamic state effects (such as attentional engagement or fatigue). Furthermore, the remaining communications could relate to the synchronisation between sender and receiver nodes that is necessary to form a carrier network to convey the feature information (Ziemer and Tranter, 2006; Lobier et al., 2014; Sherblom, 2019).

A similar logic isolated the mediatory role of PFC. Thus, DFI addressed the first question schematized in Figure 1, of the functional network of regions that dynamically (and multi-modally) propagate a prediction of visual information to the PFC that translates a prediction from auditory cortex into a predictive signal in occipital cortex that subsequently influences the representation of stimulus contents, when shown.

These Stage 2 effects were obtained from the contrast between the two auditory cues, and therefore might reflect only bottom-up processing of these auditory signals (not the predicted visual contents). However, our demonstration that PFC mediates the propagation addresses this point, by showing a high-level modulation distinct from the dynamic representation of the tone itself (tested with the localizer prior to the experiment, see Figure 7). Also, we proved the visual specificity of the Stage 2 prediction with end point in occipital cortex contra-lateral to the predicted location (cf. Figure 3). Thus, the propagation of the visual prediction at Stage 2 is distinct from that of the auditory input.

To address the question of how prediction influences Stage 3 processing of the stimulus, we compared Stage 3 stimulus representation with and without prediction. A key unresolved question about the role of predictions is whether they enhance vs. dampen stimulus representation (De Lange et al., 2018). Evidence for one or the other typically relies on enhanced vs. impaired decoding performance of the predicted stimulus in the regions of interest (Lee and Mumford, 2003; Kok et al., 2012; Blank and Davis, 2016; Kumar et al., 2017). Here, we showed that predictions enhance the representation of LSF vs. HSF stimulus contents, locating these enhancements in source space and time. Most participants (7/11) showed that prediction enhances LSF vs. HSF discrimination in occipital cortex and (9/11) in parietal cortex and (9/11) in premotor cortex, the latter relating to faster behavioral categorization. Thus, our evidence supports the hypothesis that prediction enhances stimulus representation in the Categorization Network.

*The mediation (i.e. control) role of prefrontal cortex*

An interesting finding of our functional network is that prefrontal cortex mediates the temporal to occipital communication of the predictive cue. More precisely, we located the sources with highest representation of the predictive cue in the dorsolateral prefrontal cortex (dlPFC, (Sanches et al., 2009)), often related to working memory (D'Esposito et al., 1998; Rowe et al., 2000; Friedman and Robbins, 2022), selective attention (Goddard et al., 2022) and task performance (Collette et al., 2005). Prefrontal cortex could orchestrate the information of the auditory cue (i.e. upcoming LSF vs. HSF) together with the memory of the upcoming stimulus location (i.e. left vs. right visual field) and selectively prepare the contra-lateral occipital sources to the upcoming contents. Our results are compatible with this hypothesis, because representation of the prediction on occipital sources at Stage 2 is indeed contralateral to the predicted visual field where the stimulus will appear at Stage 3—i.e. left occipital sources for a predicted right visual field stimulus and vice versa. Future work that fuses MEG and high-field fMRI will seek to resolve the specific cortical laminar layer that receives the prediction at Stage 2 (e.g. central laminar layer (Lawrence et al., 2019)), and

how this prediction then interacts with the cortical layer representation of the feedforward flow when the stimulus is shown at Stage 3 (e.g. in peripheral laminar layers (Lawrence et al., 2019)).

*Predictions and representations of face, object, body and scene stimuli.*

We used DFI to reconstruct the dynamic Prediction and Categorization Networks. Our approach to the neuroimaging of cognitive tasks differs from most other approaches in several critical ways. First, our overarching goal is to reconstruct, for each individual participant, the network of MEG sources that communicate (i.e. send and receive) the information (e.g. an auditory cue; a visual feature) that is necessary to resolve the cognitive task under study (Schyns et al., 2009, 2022; Jaworska et al., 2022). These cognitive tasks play a critical role to shape the communications of specific stimulus and memory information across the networks of the brain (Schyns, 1998; Smith et al., 2004; Jaworska et al., 2022; Schyns et al., 2022; Kay et al., 2023). Second, to do so, we use a new measure of functional connectivity (i.e. DFI (Ince et al., 2015b, 2016)) that differs from most other signal-to-signal measures of connectivity (e.g. Granger causality(Bressler and Seth, 2011) or transfer entropy(Lobier et al., 2014)). DFI quantifies communication of specific information between network nodes. For example, at Stage 2 of our Experiment, nodes communicate the information about the auditory prediction of LSF vs. HSF. DFI communication is expressed as a percentage of the full signal-to-signal connectivity between pairs of nodes. With DFI, we can uniquely interpret neural signal communications in terms of the specific information contents that the brain networks flexibly communicate to achieve a cognitive task. This is important to isolate because we showed in our prediction experiment that communications of the predicted features is only about 55%-75% of all signal-to-signal communications between brain regions. A direct consequence of DFI connectivity is that we can locate the network nodes where different information converges (i.e. the hubs–e.g. contra-lateral occipital representations of the left and right eyes of a face converge into the right fusiform gyrus hub(Schyns et al., 2007; Ince et al., 2016; Zhan et al., 2019; Jaworska et al., 2022)). In turn, we can analyze whether hub nodes perform specific linear and nonlinear computations on their inputs(Jaworska et al., 2022). And these analyses apply equally to bottom-up and top-down information flows in the network. Here, they revealed mechanisms that top-down propagate predictions of LSF vs. HSF stimulus feature, from temporal to lateralized occipital cortex, depending on task demands. In turn, these predictions enhance bottom-up LSF vs. HSF representations, from occipital cortex to pre-motor cortex, to speed up categorization behavior. Thus, our approach enables a unique mechanistic, algorithmic understanding of the information processing network that realize a specific cognitive task, which is the ultimate explanatory goal of cognitiveneuroimaging(Schyns et al., 2009, 2022; Jaworska et al., 2022).

Generalizing from Gabor stimuli to more naturalistic face, object and scene categorization tasks will incur several challenges to study the visual features that categorizes faces, objects and scenes (Schyns et al., 2009, 2020). A key challenge is that the stimulus features participants use to predict and then categorize can differ across behaviors and levels of expertise (e.g. categorizing the same picture as “city” vs. “New York”) (Gauthier et al., 1999; Malcolm et al., 2014). We therefore need to characterize these features per participant and task to then study their predictions and representations for behavior in functional networks (Jaworska et al., 2022; Schyns et al., 2022; Kay et al., 2023). In particular, a methodological challenge remains to understand the compositionality of visual predictions, as they

796 decompose from their integrated representation high in the visual hierarchy (e.g., right
797 fusiform gyrus), to their contra-lateral components for occipital cortex, down to their simplest
798 Gabor representation in the lower hierarchical levels. This would require fusion of brain
799 measures (e.g. high-field fMRI to finely tap into laminar layers (Gilbert and Li, 2013) and
800 E/MEG (Ince et al., 2015b) to trace the dynamics of these representations across layers in
801 the occipito-ventral-dorsal streams).

802 Thus, to understand complex dynamic predictions and representations in the brain, we must
803 understand the categorization task (e.g. “city vs. New York”), the hierarchical composition of
804 features that represent each category in the participant’s memory, trace their hierarchical
805 predictions in the feedback flow (Yuille and Kersten, 2006) and their subsequent
806 representation in the feedforward flow when the stimulus is shown. Once the
807 compositionality of representations is understood, we could study how sensory hierarchies
808 decompose predictions to facilitate stimulus processing and behavior.

809

## 810 Conclusions

811 We sought to isolate and understand the propagation of specific cognitive predictions in a
812 Prediction Network and then how these predictions change the Categorization Network that
813 processes the predicted contents in the stimulus. We showed that the Prediction Network
814 dynamically propagates predictions of visual contents from temporal to occipital regions, via
815 the flexible mediation role of prefrontal regions. Then, we showed that predicted contents
816 were more sharply represented when the stimulus is shown in the Categorization Network,
817 from occipital-ventral to pre-motor cortex, via parietal cortex, leading to faster decision
818 behavior. Our Prediction and Categorization Networks split the communications on specific
819 contents from overall signal-to-signal connectivity, in principle generalizing to other stimulus
820 features and sensory modalities.

821 **Reference**


822 Bar M, Kassam KS, Ghuman AS, Boshyan J, Schmid AM, Dale AM, Hämäläinen MS,
823 Marinkovic K, Schacter DL, Rosen BR (2006) Top-down facilitation of visual
824 recognition. Proc Natl Acad Sci 103:449–454.

825 Benedek M, Bergner S, Könen T, Fink A, Neubauer AC (2011) EEG alpha synchronization is
826 related to top-down processing in convergent and divergent thinking.
827 Neuropsychologia 49:3505–3511.

828 Blank H, Davis MH (2016) Prediction errors but not sharpened signals simulate multivoxel
829 fMRI patterns during speech perception. PLoS Biol 14:e1002577.

830 Bressler SL, Seth AK (2011) Wiener–Granger causality: a well established methodology.
831 Neuroimage 58:323–329.

832 Clark A (2013) Whatever next? Predictive brains, situated agents, and the future of cognitive
833 science. Behav Brain Sci 36:181–204.

834 Collette F, Olivier L, Van der Linden M, Laureys S, Delfiore G, Luxen A, Salmon E (2005)
835 Involvement of both prefrontal and inferior parietal cortex in dual-task performance.
836 Cogn Brain Res 24:237–251.

837 De Lange FP, Heilbron M, Kok P (2018) How do expectations shape perception? Trends
838 Cogn Sci 22:764–779.

839 D'Esposito M, Aguirre GK, Zarahn E, Ballard D, Shin RK, Lease J (1998) Functional MRI
840 studies of spatial and nonspatial working memory. Cogn Brain Res 7:1–13.

841 Flom MC, Heath GG, Takahashi E (1963) Contour interaction and visual resolution:
842 Contralateral effects. Science 142:979–980.

843 Friedman NP, Robbins TW (2022) The role of prefrontal cortex in cognitive control and
844 executive function. Neuropsychopharmacology 47:72–89.

845 Friston K (2010) The free-energy principle: a unified brain theory? Nat Rev Neurosci 11:127–
846 138.

847 Gauthier I, Tarr MJ, Anderson AW, Skudlarski P, Gore JC (1999) Activation of the middle
848 fusiform'face area'increases with expertise in recognizing novel objects. Nat Neurosci
849 2:568–573.

850 Gilbert CD, Li W (2013) Top-down influences on visual processing. Nat Rev Neurosci 14:350.

851 Gilbert CD, Sigman M (2007) Brain States: Top-Down Influences in Sensory Processing.
852 Neuron 54:677–696.

853 Goddard E, Carlson TA, Woolgar A (2022) Spatial and Feature-selective Attention Have
854 Distinct, Interacting Effects on Population-level Tuning. J Cogn Neurosci 34:290–312.

855 Gross J (2019) Magnetoencephalography in cognitive neuroscience: a primer. Neuron
856 104:189–204.

857 Haegens S, Händel BF, Jensen O (2011) Top-down controlled alpha band activity in
858 somatosensory areas determines behavioral performance in a discrimination task. J
859 Neurosci 31:5197–5204.

860 Hindy NC, Ng FY, Turk-Browne NB (2016) Linking pattern completion in the hippocampus to
861 predictive coding in visual cortex. Nat Neurosci 19:665–667.

862 Ince RA, Giordano BL, Kayser C, Rousselet GA, Gross J, Schyns PG (2017) A statistical
863 framework for neuroimaging data analysis based on mutual information estimated via
864 a gaussian copula. Hum Brain Mapp 38:1541–1573.

865 Ince RA, Jaworska K, Gross J, Panzeri S, Van Rijsbergen NJ, Rousselet GA, Schyns PG
866 (2016) The deceptively simple N170 reflects network information processing
867 mechanisms involving visual feature coding and transfer across hemispheres. Cereb
868 Cortex 26:4123–4135.

869 Ince RA, Paton AT, Kay JW, Schyns PG (2021a) Bayesian inference of population
870 prevalence. Elife 10:e62461.

871 Ince RA, Paton AT, Kay JW, Schyns PG (2021b) Bayesian inference of population
872 prevalence. bioRxiv:2020.07. 08.191106.

873 Ince RA, Van Rijsbergen NJ, Thut G, Rousselet GA, Gross J, Panzeri S, Schyns PG (2015a)
874 Tracing the flow of perceptual features in an algorithmic brain network. Sci Rep 5:1–
875 17.

876 Ince RAA, Kay JW, Schyns PG (2022) Within-participant statistics for cognitive science.
877 Trends Cogn Sci Available at:
878 https://www.sciencedirect.com/science/article/pii/S1364661322001140.

879 Ince RAA, van Rijsbergen NJ, Thut G, Rousselet GA, Gross J, Panzeri S, Schyns PG
880 (2015b) Tracing the Flow of Perceptual Features in an Algorithmic Brain Network. Sci
881 Rep 5:17681.

882 Jaworska K, Yan Y, Van Rijsbergen NJ, Ince RA, Schyns PG (2022) Different computations
883 over the same inputs produce selective behavior in algorithmic brain networks. Elife
884 11:e73651.

885 Kay K, Bonnen K, Denison RN, Arcaro MJ, Barack DL (2023) Tasks and their role in visual
886 neuroscience. Neuron Available at:
887 https://www.sciencedirect.com/science/article/pii/S0896627323002180.

888 Kinchla RA, Wolfe JM (1979) The order of visual processing:“Top-down,”“bottom-up,” or
889 “middle-out.” Percept Psychophys 25:225–231.

890 Kok P, Failing MF, de Lange FP (2014) Prior expectations evoke stimulus templates in the
891 primary visual cortex. J Cogn Neurosci 26:1546–1554.

892 Kok P, Jehee JFM, de Lange FP (2012) Less Is More: Expectation Sharpens
893 Representations in the Primary Visual Cortex. Neuron 75:265–270.

894 Kok P, Mostert P, De Lange FP (2017) Prior expectations induce prestimulus sensory
895 templates. Proc Natl Acad Sci 114:10473–10478.

Kumar S, Kaposvari P, Vogels R (2017) Encoding of predictable and unpredictable stimuli by inferior temporal cortical neurons. J Cogn Neurosci 29:1445–1454.

Lawrence SJ, Formisano E, Muckli L, de Lange FP (2019) Laminar fMRI: Applications for cognitive neuroscience. Neuroimage 197:785–791.

Lee TS, Mumford D (2003) Hierarchical Bayesian inference in the visual cortex. JOSA A 20:1434–1448.

Lobier M, Palva JM, Palva S (2018) High-alpha band synchronization across frontal, parietal and visual cortex mediates behavioral and neuronal effects of visuospatial attention. NeuroImage 165:222–237.

Lobier M, Siebenhühner F, Palva S, Palva JM (2014) Phase transfer entropy: a novel phase-based measure for directed connectivity in networks coupled by oscillatory interactions. Neuroimage 85:853–872.

Malcolm GL, Nuthmann A, Schyns PG (2014) Beyond gist: Strategic and incremental information accumulation for scene categorization. Psychol Sci 25:1087–1097.

Margalit E, Jamison KW, Weiner KS, Vizioli L, Zhang R-Y, Kay KN, Grill-Spector K (2020) Ultra-high-resolution fMRI of human ventral temporal cortex reveals differential representation of categories and domains. J Neurosci 40:3008–3024.

Massey J (1990) Causality, feedback and directed information. In, pp 303–305.

Michalareas G, Vezoli J, Van Pelt S, Schoffelen J-M, Kennedy H, Fries P (2016) Alpha-beta and gamma rhythms subserve feedback and feedforward influences among human visual cortical areas. Neuron 89:384–397.

Oostenveld R, Fries P, Maris E, Schoffelen J-M (2011) FieldTrip: open source software for advanced analysis of MEG, EEG, and invasive electrophysiological data. Comput Intell Neurosci 2011.

Posner MI, Petersen SE (1990) The attention system of the human brain. Annu Rev Neurosci 13:25–42.

Rowe JB, Toni I, Josephs O, Frackowiak RS, Passingham RE (2000) The prefrontal cortex: response selection or maintenance within working memory? Science 288:1656–1660.

Sanches M, Caetano S, Nicoletti M, Monkul ES, Chen HH, Hatch JP, Yeh P-H, Mullis RL, Keshavan MS, Rajowska G, Soares JC (2009) An MRI-based approach for the measurement of the dorsolateral prefrontal cortex in humans. Psychiatry Res 173:150–154.

Schyns PG (1998) Diagnostic recognition: task constraints, object information, and their interactions. Cognition 67:147–179.

Schyns PG, Gosselin F, Smith ML (2009) Information processing algorithms in the brain. Trends Cogn Sci 13:20–26.

Schyns PG, Petro LS, Smith ML (2007) Dynamics of visual information integration in the brain for categorizing facial expressions. Curr Biol 17:1580–1585.

934 Schyns PG, Snoek L, Daube C (2022) Degrees of algorithmic equivalence between the brain
935 and its DNN models. Trends Cogn Sci.

936 Schyns PG, Zhan J, Jack RE, Ince RA (2020) Revealing the information contents of memory
937 within the stimulus information representation framework. Philos Trans R Soc B
938 375:20190705.

939 Sherblom JC (2019) Computer-Mediated Communication: Approaches and Perspectives.
940 Cognella, Incorporated.

941 Smith ML, Gosselin F, Schyns PG (2004) Receptive fields for flexible face categorizations.
942 Psychol Sci 15:753–761.

943 Smith SM, Nichols TE (2009) Threshold-free cluster enhancement: addressing problems of
944 smoothing, threshold dependence and localisation in cluster inference. Neuroimage
945 44:83–98.

946 Treder MS (2020) MVPA-Light: a classification and regression toolbox for multi-dimensional
947 data. Front Neurosci 14:289.

948 Yuille A, Kersten D (2006) Vision as Bayesian inference: analysis by synthesis? Trends
949 Cogn Sci 10:301–308.

950 Zhan J, Ince RA, Van Rijsbergen N, Schyns PG (2019) Dynamic construction of reduced
951 representations in the brain for perceptual decision behavior. Curr Biol 29:319-326.
952 e4.

953 Ziemer R, Tranter WH (2006) Principles of communications: system modulation and noise.
954 John Wiley & Sons.

955

# Figure Legends

**Figure 1. Three key questions. 1) Prediction Network:** Where, when and how does it flexibly represent and communicate a predictive cue depending on task demands (here P, an auditory cue that predicts a visual content). **2) Categorization network:** When, where and how does it process the stimulus contents (here S, the LSF vs. HSF of a Gabor stimulus)? **3) Influence of prediction on categorization:** How does content prediction influence stimulus representation, leading to faster behavior?

**Figure 2. Experimental design and behavioral results. (A) Task procedure.** Each trial started with a 500ms fixation. At Stage 1, a 100ms green dot (i.e. location cue) predicted the left vs. right task-demand location of the upcoming Gabor patch, followed by 1000-1500ms blank screen. At Stage 2, a 250ms sweeping sound (i.e., SF cue) predicted the LSF vs. HSF content of the upcoming Gabor, followed by a 1000-1500ms blank screen with jitter. At Stage 3, the Gabor stimulus was presented for 100ms. Participants categorized its LSF vs. HSF, followed by a 750-1250ms inter-trial interval (ITI). **(B) Cue-Gabor couplings.** At Stage 1, the left vs. right location cue predicted the left vs. right location of the upcoming Gabor with 100% validity. At Stage 2, on predictive trials, the 196 Hz vs. 2217 Hz auditory cues predicted the Gabor LSF vs. HSF contents with 90% validity; on neutral trials, a 622 Hz auditory cue served as neutral control on 33% of the trials contained no prediction (i.e. with .5 probability of LSF vs. HSF). **(C) Behavioral results.** Boxplots show that prediction (i.e., valid predictive cueing, dark brown) sped up median LSF vs. HSF Gabor categorization RTs in left and right-cued trials, compared with neutral cueing (light brown). Black dots (vs. light grey dots) indicate the per-participant median categorization RTs in predictive (vs. neutral) trials, linked to show directional RT differences replicated in each individual participant.

**Figure 3. Stage 2 Prediction Network. (A) Network regions (see iconic brain).** In each participant, we computed the Stage 2 prediction representation (as MI(LSF vs. HSF cue; $MEG_t$), Y-axis), between 0 and 0.4s post auditory cue (X-axis), on each source, separately for left- and right-cued trials (see *Methods, Prediction representations*). We then localized the single source with maximum MI value in each color-coded period—i.e. [90-120ms], [120-200ms], [>200ms], see *Methods, Prediction Network, Prediction periods clustering.* Glass brains show the cross-participant mean of maximum MI for these sources, revealing a temporal sequence of prediction representation propagation from temporal (TL, cyan) to prefrontal (PFC, magenta) to occipital (orange, contra-laterally to the left vs. right cued stimulus location lOC vs. rOC). **(B) Prediction communications.** For each participant, we used these three sources (i.e. one per color-coded period) as the three functional nodes to reconstruct their Prediction Network. With DFI (Ince et al., 2015a) we computed the Stage 2 communications of the prediction across these three network nodes—i.e. TL->PFC and PFC->OC. Plots show these communications averaged across participants, in the time course of the receiving node (X-axis), as delays from the sending node (Y-axis)–e.g. TL sends predictive cue P to PFC, with a 50ms delay, then PFC sends P to OC, with a 100-200ms delay (as illustrated in the iconic brain below).

**Figure 4. Prefrontal cortex mediates prediction communication. (A) Direct communication** of the prediction from TL to OC, illustrated in a typical participant. We removed (i.e. conditioned out) the mediation role of PFC in communicating prediction P between TL and lateralized left (l) or right (r) OC. The matrices express these P communications in the time course of the receiving lOC source (X-axis), as delays from the sending TL source (Y-axis). **(B) Prefrontal mediation** in communicating P from TL to lOC, with a 100-150 ms delay, illustrated in a typical participant. The significant difference between

(A) Direct and (B) Mediated communications is indicated with a red solid curve in the participant plot (right-cued trials, FWER corrected, $p$<0.05, one-tail). **(C) Group generalization.** The plot shows the cross-participant mean significant difference between (A) Direct and (B) Mediated prediction communication for right-cued trials. The effect replicated in 11/11 participants for left-cued trials (FWER corrected, $p$<0.05, one-tail), Bayesian population prevalence = 1 [0.77 1] MAP [95% HPDI], and in 10/11 participants for right-cued trials, Bayesian population prevalence = 0.91 [0.64 0.99], MAP [95% HPDI]. PFC therefore actively mediates network communications of P from TL to lateralized OC.

**Figure 5. Stage 3 Categorization Network. (A) Network regions (see iconic brain).** In each participant, we computed the Stage 3 Gabor stimulus LSF vs. HSF representation (as MI(LSF vs. HSF Gabor; $MEG_t$), Y-axis), between 0 and 0.5s post stimulus (X-axis) on each source, separately for left- and right-cued trials. We then localized the single source with maximum MI value in each color-coded period—i.e. [150-250 ms], [250-350 ms], [>350 ms]. Glass brains shows the cross-participant mean of maximum MI for these sources, revealing the temporal sequence of stimulus representation propagation starting in contra-lateral occipital-ventral cortex (OC, orange), then parietal lobe (PL, red), and finally premotor and frontal cortex (PMC, brown), independently for left- and right-cued trials. **(B) Stimulus communications**. For each participant, we used these three sources (one per color-coded period) as the three functional sources to reconstruct their Categorization Network. With DFI (Ince et al., 2015a), we computed the Stage 3 communications of Gabor stimulus across these three network nodes—i.e. OC->PL->PMC. Plots show these communications averaged across participants, in the time course of the receiving node (X-axis), as delays from the sending node (Y-axis)–e.g. lOC sends stimulus S contents to PL, with a 100 ms delay (as illustrated in the iconic brain plots below).

**Figure 6. Interaction between Prediction Network (Stage 2) and Categorization Network (Stage 3). (A) Does prediction enhance SF discrimination for categorization?** Boxplots comprise the highest per participant source-level difference of Stage 3 stimulus SF representation–i.e. difference of MI(LSF vs. HSF; $MEG_{Stage3}$) for valid predictive vs. no prediction trials against the null hypothesis of no difference, FWER, $p$<0.05, two-tailed, in each color-coded region and time window (contra-lateral occipital-ventral: 150-250ms; parietal: 250-350ms; PMC: >350ms). These representational enhancements of stimulus SF replicate in each region and time window (see prevalence bar adjacent to boxplots, for left- and right-cued trials). **(B) Where and when does prediction speed up behavioral RT in the Categorization Network?** To identify the Stage 3 Categorization Network regions whose sources relate to faster RTs following valid predictions (vs. no prediction), we computed Co-I(Predictive vs. neutral trials; $MEG_{Stage3}$; RT), FWER-corrected, $p$<0.05, separately for left- (dashed line) and right-cued trials (plain line) on all Stage 3 Categorization Network sources (contra-lateral occipital cortex, parietal lobe and premotor cortex). Plain (right-cued trials) and dashed left-cued trials) curves plot the averages of the per-participant maximum Co-I across sources at each time point. They reveal two sequential peaks post ~250ms, in parietal lobe and pre-motor cortex. Small locate shows the mean Co-I of the individual participant sources that contribute to these peaks.

**Figure 7. Control analyses for Stage 2. (A) Dot representation before auditory cue onset.** For each individual participant, we computed the representation of the dot cue (as MI(left vs. right dot; $MEG_t$), Y-axis). We computed the trial-by-trial dot cue representation, by computing MI(<left vs. right dot; Stage 1 MEGt>), at each 4ms time point between 0 to 1000 ms following Stage 1 dot cue onset, and also each at time point from -100ms to 0ms before Stage 2 auditory cue onset, on each source in lingual gyrus, cuneus and inferior occipital gyrus. We then averaged time courses of dot representation across the sources. Results show the dot representation ceases prior to the onset of auditory cues. **(B) Auditory processing decoding.** Curves show the auditory decoding performance of the LSF vs. HSF cue, separately for left-cued (upper panel) and right-cued (lower panel) conditions.

We trained classifiers on the auditory localizer to discriminate LSF vs. HSF cue, every 2ms between 0 and 400ms; and tested these classifiers on Stage 2, every 2ms between 0 and 400ms. We quantified the decoding performance (FWER-corrected, $p<0.05$, one-tailed) as MI (classifier decision value; ground truth LSF vs. HSF cue), and took the highest significant performance across training time points. The curve shows the averaged decoding performance across participants – shaded regions denote ± standard errors of the mean. Cortical surface maps reveal the MEG sources that contribute to the decoding peaks in each time window of the prediction dynamics, computed as MI(classifier decision value; MEG source activity), indicating the source representation of the auditory cues remains within TL from left hemisphere to the right.

**Figure 8. Stage 2: Communications (DFI) of the LSF vs. HSF prediction in the Prediction Network of individual participants.** Using DFI, separately for **(A) left-cued trials** and **(B) right-cued trials**, we computed in each participant (each grey-framed panel) the communications of the prediction across network nodes (i.e. TL -> PFC and PFC -> OC), every 2 ms between 0 and 400ms post auditory cue onset for the receiver, and every 2 ms communication delay between 0 and 300ms from the sender. These time x time plots represent the significant (FWER-corrected, p<0.05) prediction communications between receiver (X-axis) and sender (Y-axis), where a green diagonal indicates the timing and duration of the prediction communications.

**Figure 9. Stage 2: PFC mediation of prediction communications in the Prediction Network of each participant.** Separately for **(A)** left- and **(B)** right-cued trials, we computed the difference of TL to OC Stage 2 prediction communication, between direct (removing frontal mediation) and mediated (with frontal mediation) DFI (for each receiver time point every 2 ms between 0 and 400ms post auditory cue onset, and for each sender communication delay every 2 ms between 0 and 300ms). Each plot presents the significant (FWER-corrected, p<0.05, one-tailed) PFC-mediated Stage communication of the cue between TL(Y-axis) and OC (X-axis).

**Figure 10: Stage 3: Communications (DFI) of the LSF vs. HSF Gabor stimulus in the Categorization Network of each participant.** Separately for **(A)** left- and **(B)** right-cued trials, we computed in each participant (each grey-framed panel) the DFI communications between categorization network nodes OC -> PL and PL -> PMC, every 2ms between 0 and 500ms post Gabor onset for the receiver, and for sender communication delays every 2ms between 0 and 300ms. Each plot presents the significant (FWER-corrected, p<0.05) communications of LSF vs. HSF Gabor stimulus between receiver (X-axis) and sender (Y-axis).

**Table 1.** Stimulus repetition in one cueing-categorization block

| | Location cue | SF cue | Visual stimuli (random from 3 orientations) |
|---|---|---|---|
| Repetitions/type | 27 left cues | 9 LSF cues | 8 left-LSF + 1 left-HSF |
| | | 9 HSF cues | 8 left-HSF + 1 left-LSF |
| | | 9 neutral cues | 9 left-random LSF/HSF |
| | 27 right cues | 9 LSF cues | 8 right-LSF + 1 right-HSF |
| | | 9 HSF cues | 8 right-HSF + 1 right-LSF |
| | | 9 neutral cues | 9 right-random LSF/HSF |
| Sum | 54 | | |

**Table 2.** Group-level effect of cueing on mean LSF vs. HSF, left- and right-cued Gabor categorization RTs (paired samples t-tests).

| Gabor type | RT (valid predictive, ms) | RT (neutral, ms) | RT Improvement (ms) | *t* value | *p* value |
|---|---|---|---|---|---|
| Left LSF | 530.9 | 456.8 | 74.1 | $t_{(10)} = 3.60$ | $p = 0.005$ |
| Left HSF | 555.4 | 447.7 | 107.7 | $t_{(10)} = 5.87$ | $p = 0.0002$ |
| Right LSF | 556.3 | 483.6 | 72.6 | $t_{(10)} = 3.37$ | $p = 0.007$ |
| Right HSF | 525.9 | 429.5 | 96.4 | $t_{(10)} = 4.82$ | $p = 0.0007$ |

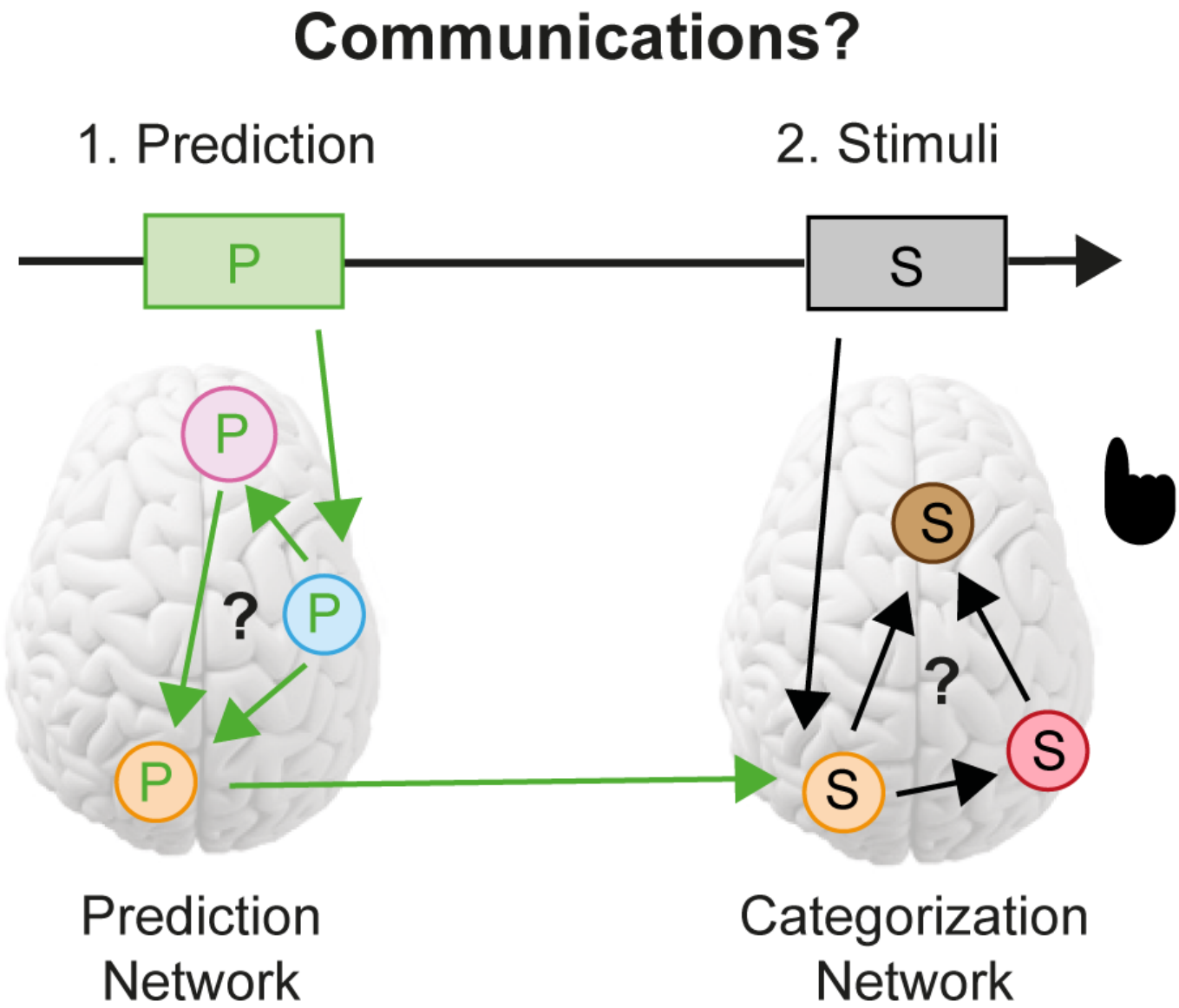

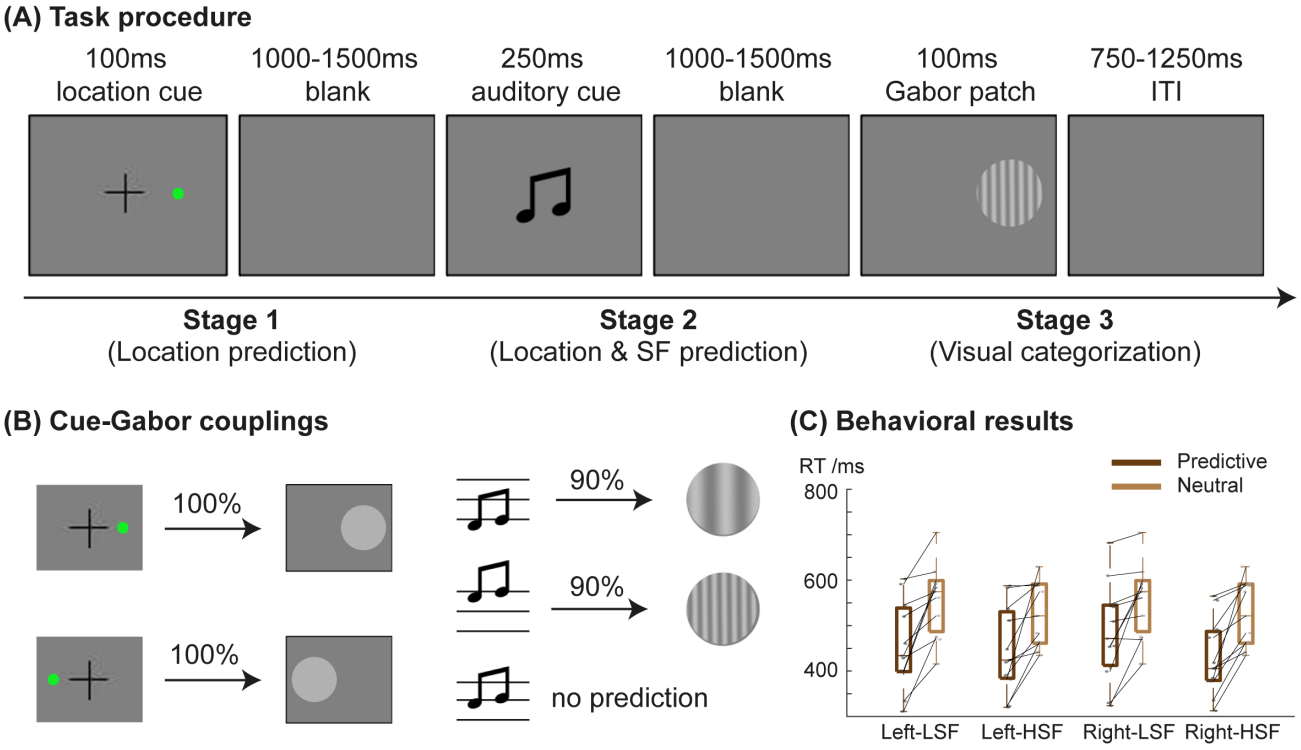

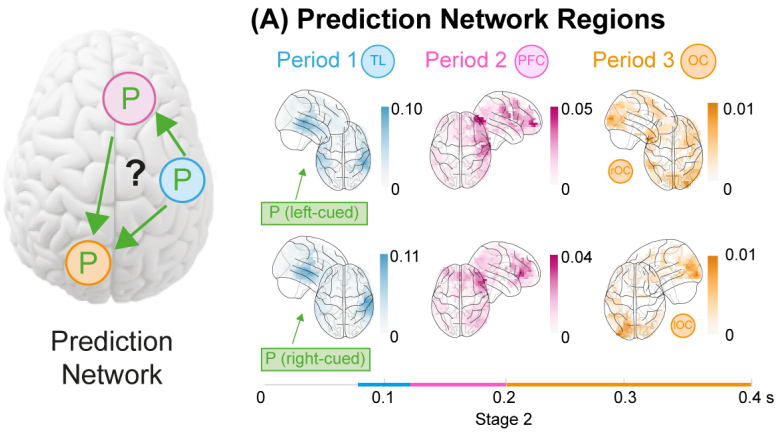

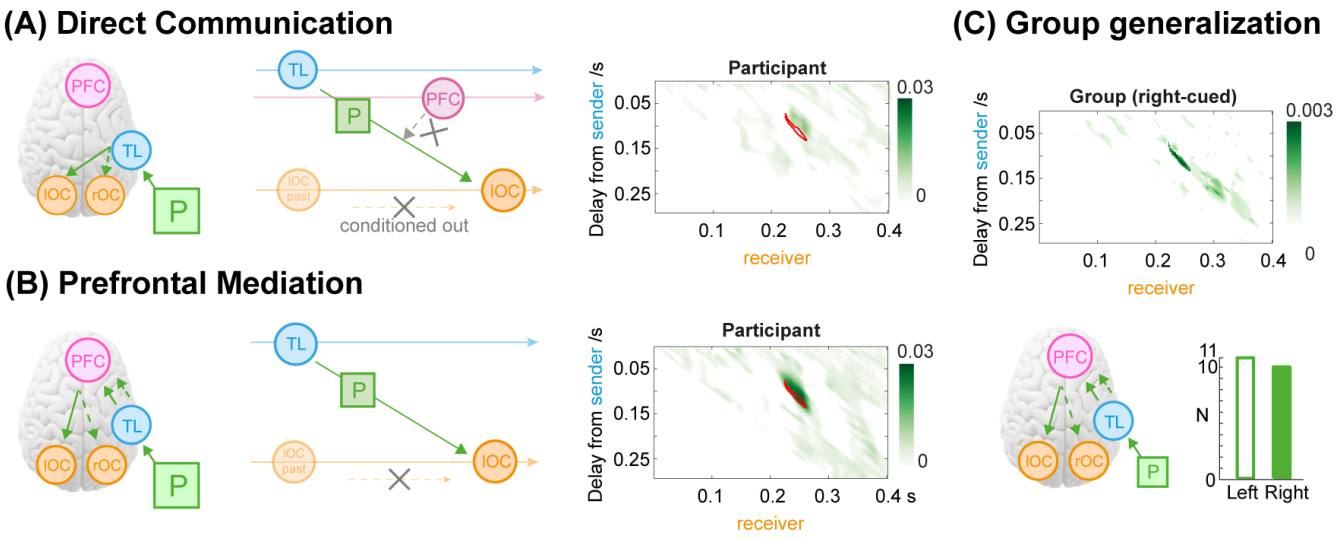

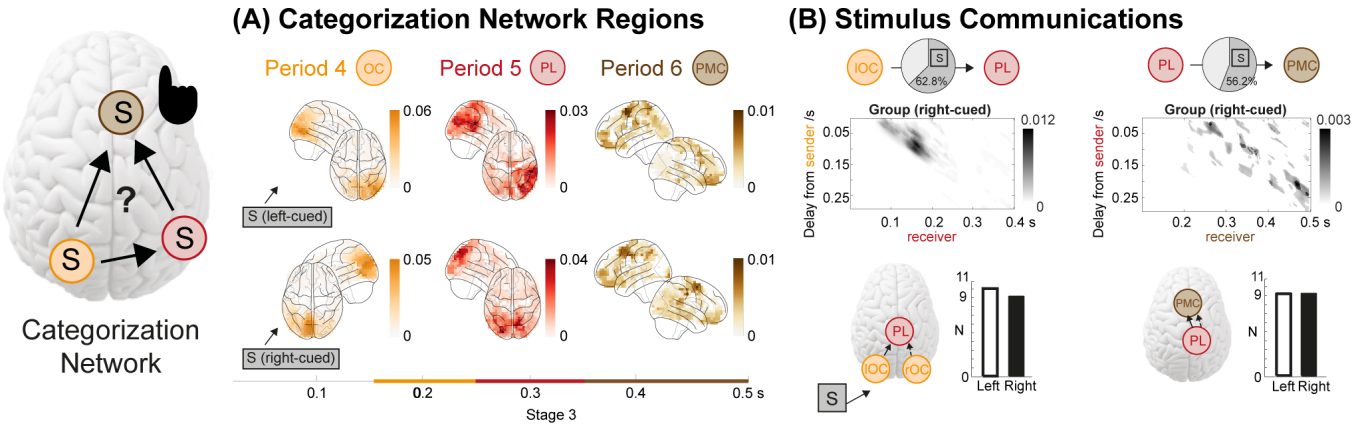

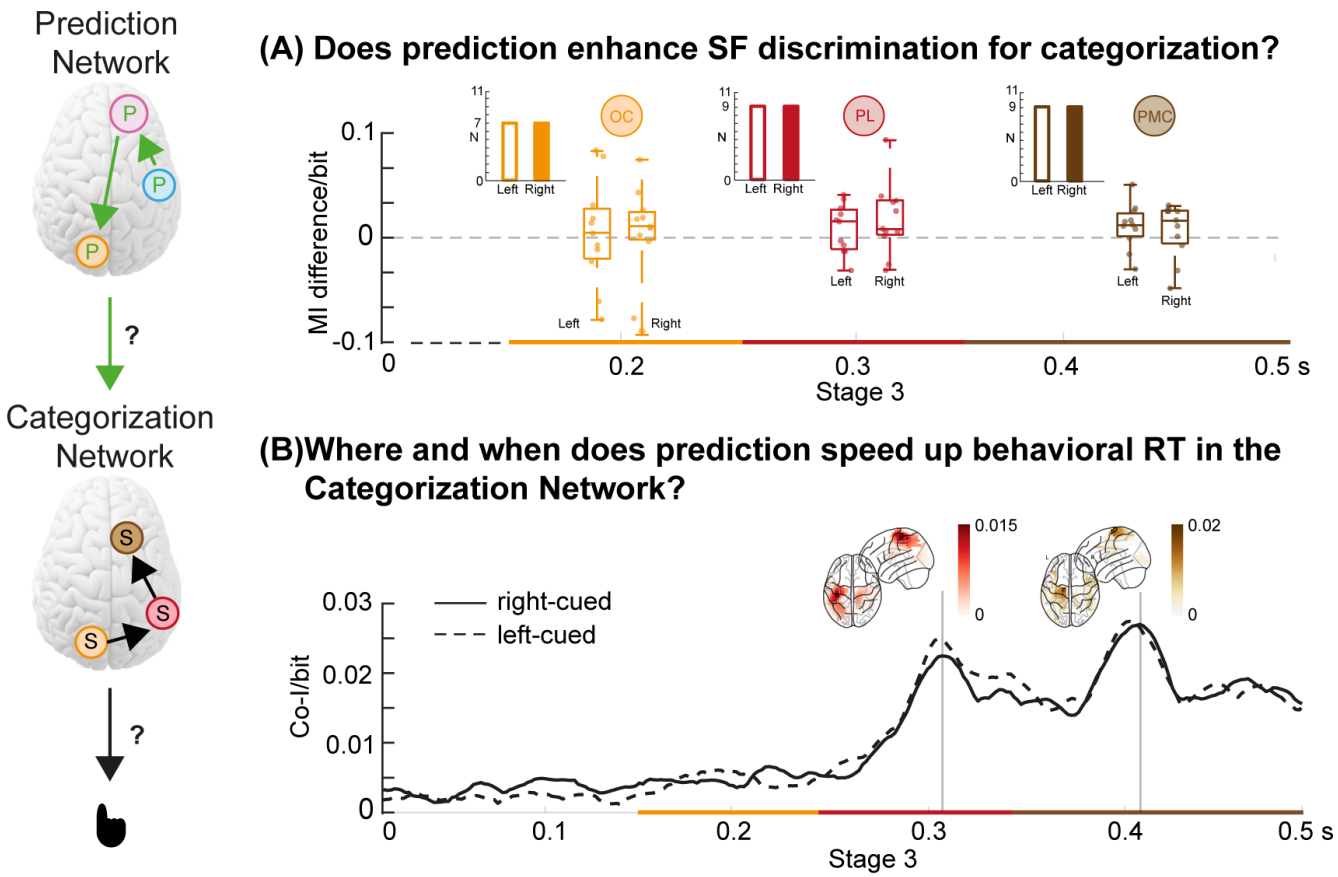

**(A) Stage 1 dot representation**

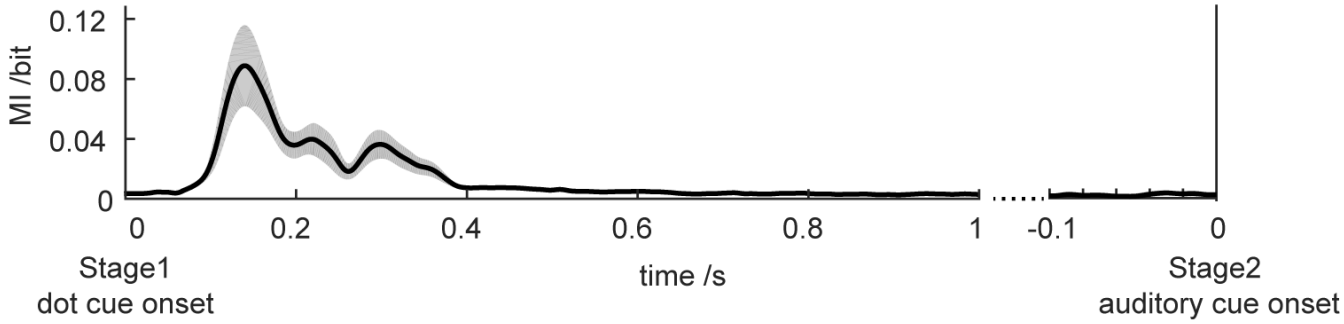


**(B) Auditory processing decoding**

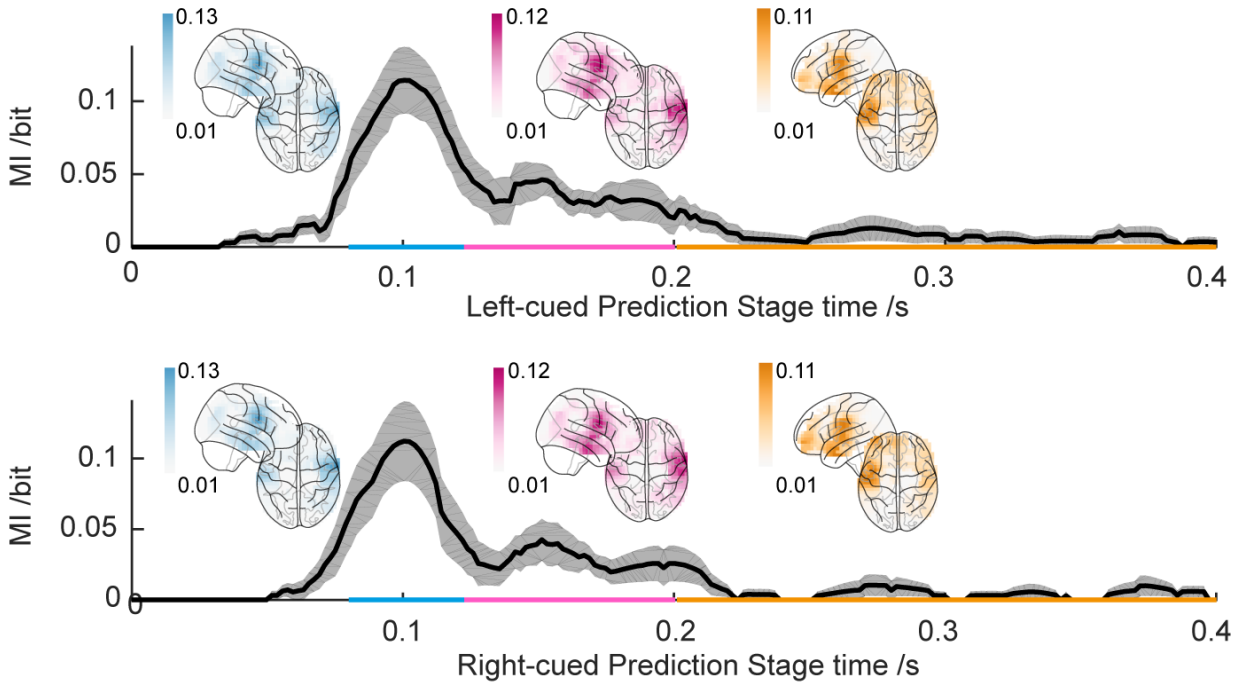

**(A) Stage 2 DFI (left-cued trials)**

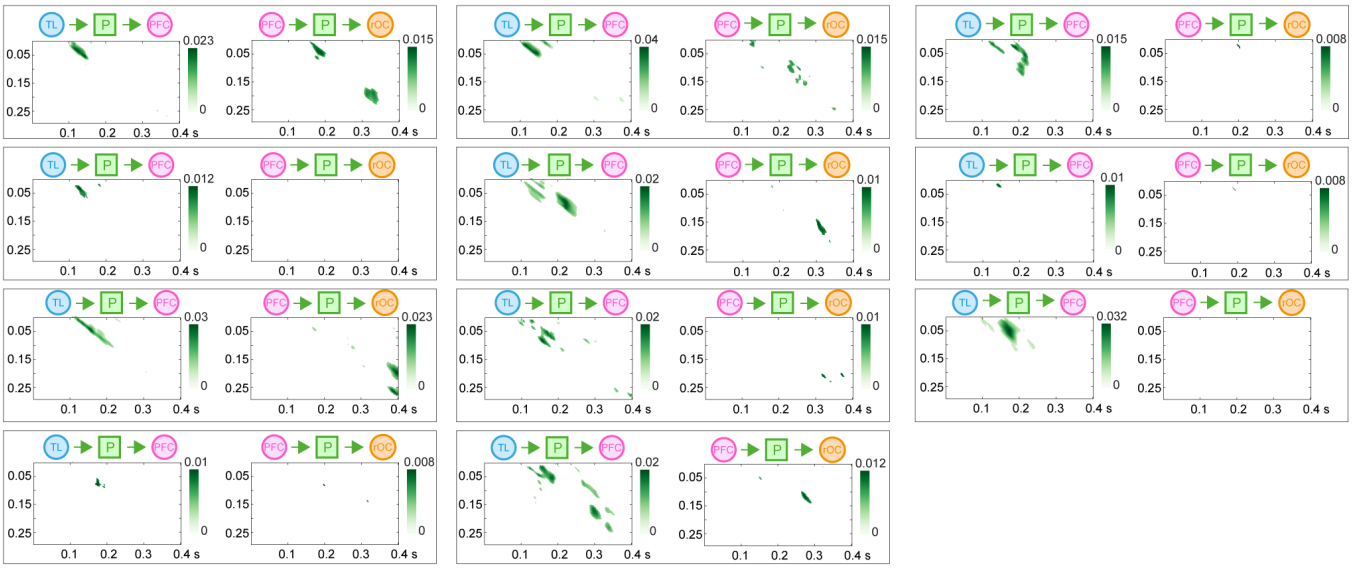


**(B) Stage 2 DFI (right-cued trials)**

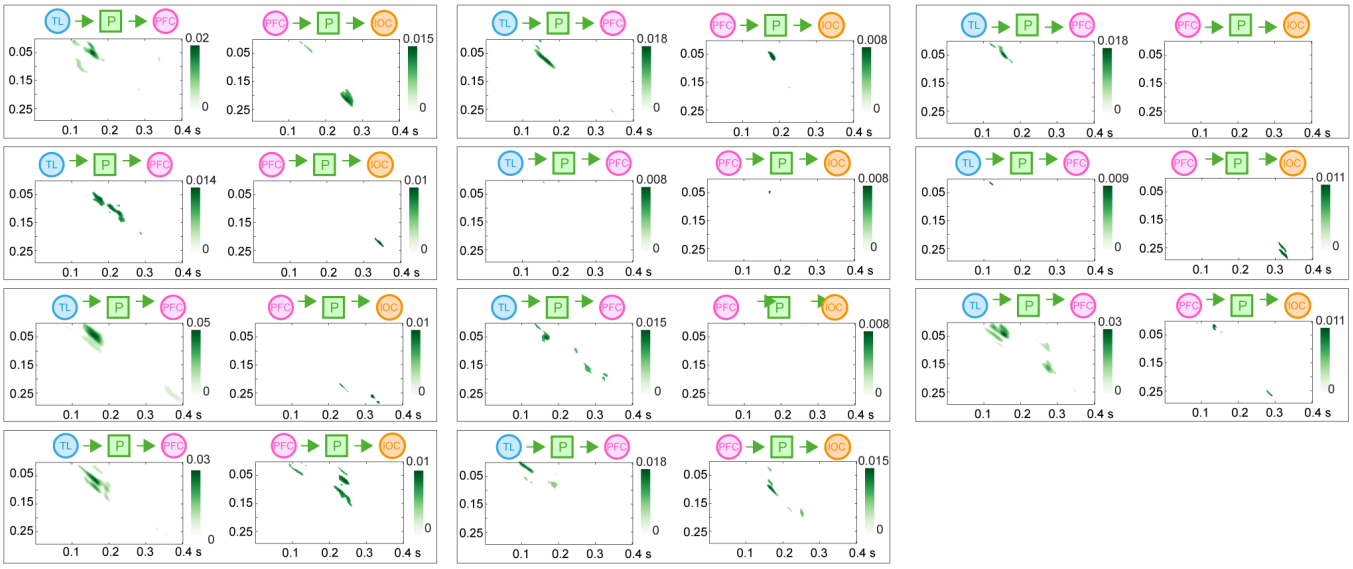

**(A) Stage 2 PFC mediation of prediction communication (left-cued trials)**

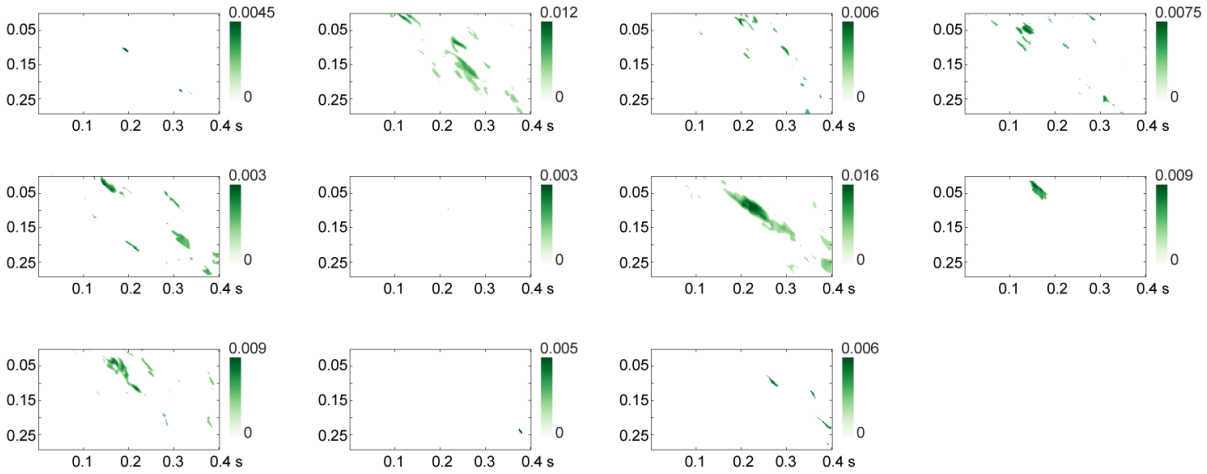


**(B) Stage 2 PFC mediation of prediction communication (right-cued trials)**

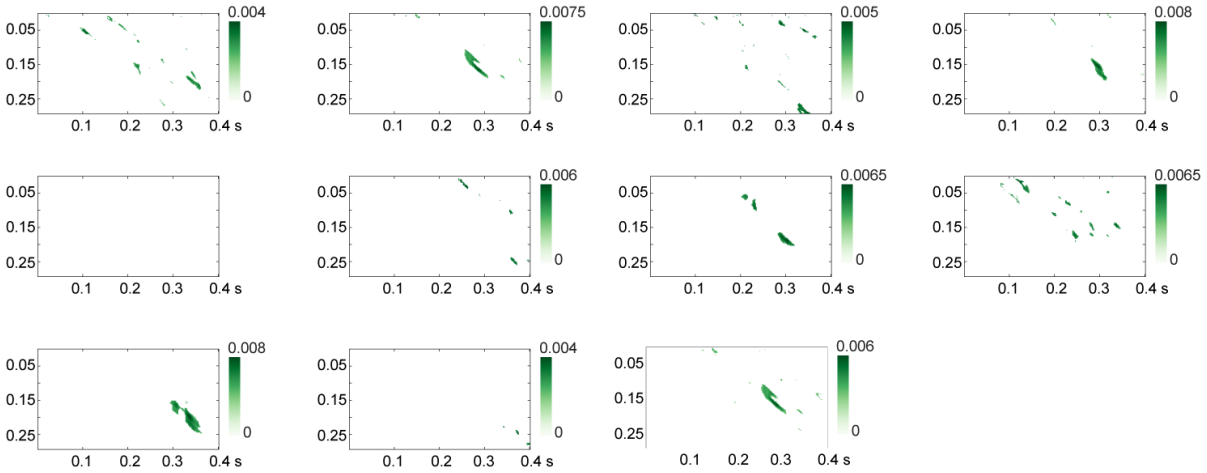

## (A) Stage 3 DFI (left-cued trials)

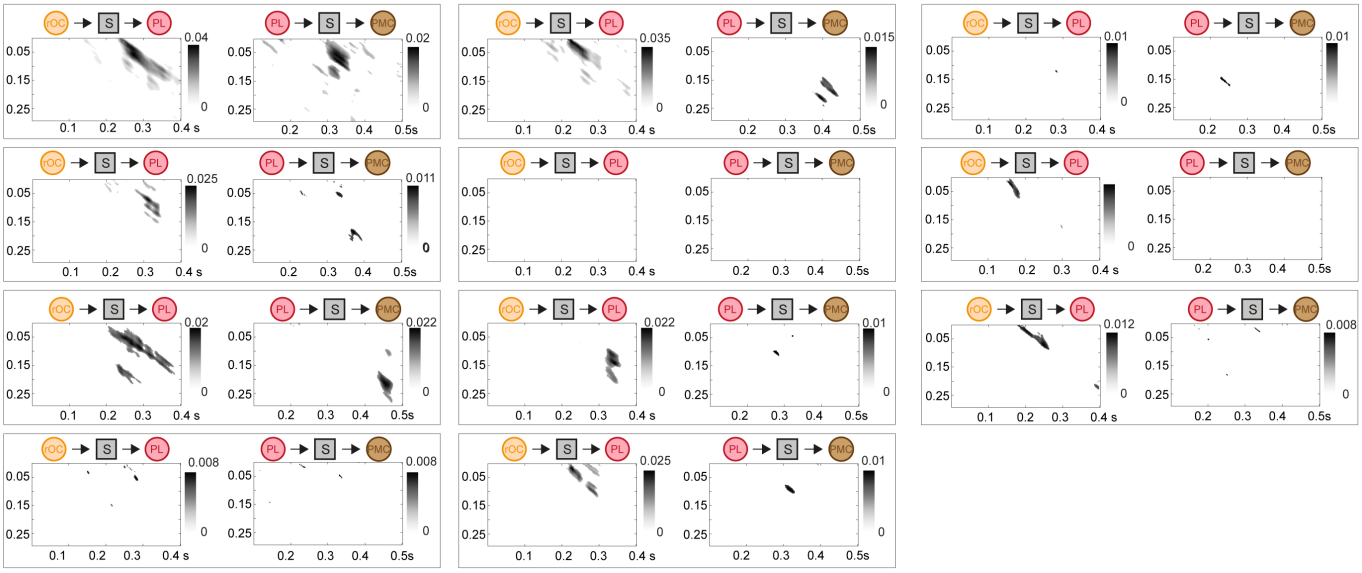

## (B) Stage 3 DFI (right-cued trials)